**National Recovery and Resilience Plan (NRRP)**

Mission 4, Component 2 (M4C2) – Investment 1.1: Fund for the National Research Programme (NRP) and Research Projects of Significant National Relevance (PRIN)

*Call PRIN 2022 PNRR – Directorial Decree no.1409, 14/09/2022*

**SubRISK+**

*Enhancing our understanding of Subsidence RISK induced by groundwater exploitation towards sustainable urban development*

CUP: B53D23033400001

DEL 3.3

**Driving and condition factors of the land subsidence in Emilia-Romagna region**

Authors:  R. Bonì, L. Goliraeisi, S. Sapio, A. Taramelli (IUSS), F. Cigna, R. Paranunzio (CNR-ISAC), P. Teatini (UNIPD)

Version 1.0, Issue date: 31/01/2025

Dissemination level: Public

## How to cite this document

BONÌ R., GOLIRAEISI L., SAPIO S., TARAMELLI A., CIGNA F., PARANUNZIO R. & TEATINI P. (2025). *PRIN 2022 PNRR SubRISK+ Deliverable DEL 3.3: Driving and condition factors of the land subsidence in Emilia-Romagna region*, Version 1.0, Issue date: 31/01/2025, pp. 53. Public Report. Available at: https://www.subrisk.eu/deliverables

## Acknowledgements

## Revision history

| Revision no. | Authors | Date | Description |
|---|---|---|---|
| 1.0 | BONÌ R., GOLIRAEISI L., SAPIO S., TARAMELLI A., CIGNA F., PARANUNZIO R. & TEATINI P. | 31/01/2025 | First release |
|  |  |  |  |
|  |  |  |  |

# Executive summary

This report summarizes the results of SubRISK+ Work Package (WP) n.3 (*WP3: Regional scale land subsidence analysis*), aimed to 1) identify subsidence hotspots, 2) interpret the drivers of the movements, and 3) assess the risk for the Emilia-Romagna region. The analysis has been performed for Emilia-Romagna, an Italian region where land subsidence has reached alarming levels, forcing regional and local authorities to take legislative measures aimed to control the process (law, 10 December 1980, n. 845).

The main input data to detect the hotspot of the land movement and assess the hazard include the Interferometric synthetic aperture radar (InSAR) datasets from Copernicus European Ground Motion Service (EGMS, https://land.copernicus.eu/en/products/european-ground-motion-service). The interpretation of the phenomena is performed using additional data such as geological and hydrogeological datasets available via the geoportal of the Emilia-Romagna region and the Regional Agency for Prevention, Environment and Energy of Emilia-Romagna (ARPAE).

Over an investigated area of more than 10,000 km$^2$, about 1,287 km$^2$ are characterised by significant land displacement over the period from 2018 to 2022. The detected displacement pattern shows a different spatio-temporal distribution in the study area. Three main independent components have been identified by analysing the displacement time series with advanced statistical methods: linear trends, non-linear trends, and seasonal movements. The first component characterizes mainly the city of Bologna; the second and third ones are detected in the proximity of the Apennine alluvial fans and in the Ravenna province, respectively.

Different drivers of the movements have been investigated, such as tectonics, soft soil compaction, groundwater withdrawal, infrastructural loading, hydrocarbon storage, and production.

A refinement of the differential displacement risk map produced at the national level (in WP2) is obtained by exploiting the building footprint database provided by the Emilia-Romagna region. The proposed approach allows for the distinction of four risk levels ranging from low to very high. A medium risk level was identified across almost 227.3 km$^2$ built-up areas of the region and a low-risk level across the remaining 71.6 km$^2$.

The generated maps provide a land subsidence hotspots database [DEL3.1] and a digital differential displacement risk map for the Emilia-Romagna region [DEL3.2]. These findings would be relevant to various stakeholders, such as regional land management and urban authorities.

# Contents

# 1. INTRODUCTION

*SubRISK+: Enhancing our understanding of Subsidence RISK induced by groundwater exploitation towards sustainable urban development* is a collaborative two years research project funded in 2023 in the framework of the Italian National Recovery and Resilience Plan (NRRP), Mission 4, Component 2 (M4C2) – Investment 1.1: Fund for the National Research Programme (NRP) and Research Projects of Significant National Relevance (PRIN) [Call "PRIN 2022 PNRR", D.D. no.1409, 14/09/2022], and led by the National Research Council (CNR) of Italy – Institute of Atmospheric Sciences and Climate (ISAC), in collaboration with the University School for Advanced Studies (IUSS) of Pavia – Department of Science, Technology and Society (STS), and the University of Padua (UNIPD) – Department of Civil, Environmental and Architectural Engineering (ICEA).

This report summarizes the results of SubRISK+ Work Package (WP) n.3 (*WP3: Regional scale land subsidence analysis*), aimed to 1) identify land subsidence hotspots, 2) interpret the drivers of the movements, and 3) assess the differential displacement risk for the plain area of the Emilia-Romagna region.

In particular, section 2 describes the input datasets used (section 2.1) and the developed methodology (section 2.2). The achieved results are then presented in section 3, which provides: the detection of the land subsidence hotspots (section 3.1), the drivers of the phenomena (section 3.2) and the differential displacement risk for the Emilia-Romagna region (section 3.3).

The digital versions of the value-added hotspot of the land subsidence and risk map for the Emilia-Romagna region are available through SubRISK+ project website within the '*Control Room*' (https://controlroom.subrisk.eu), which enables open access to SubRISK+ mapping products.

# 2. DATA & METHODS

## 2.1. Input datasets

The input datasets of the analysis include: (i) geological datasets of the Emilia-Romagna geoportal (https://geoportale.regione.emilia-romagna.it/download), (2) the hydrogeological data provided by the Regional Agency for Prevention, Environment and Energy of Emilia-Romagna (Arpae), Italy (https://www.arpae.it/it/temi-ambientali/acqua/dati-acque/acque-sotterranee/rete-di-monitoraggio-acque-sotterranee/il-monitoraggio-quantitativo-delle-acque-sotterranee), (iii) the ground displacement observations derived from the Copernicus European Ground Motion Service (EGMS) (https://egms.land.copernicus.eu/), and the (iv) urban settlement information derived from global databases and a dataset provided by the Emilia-Romagna region.

Each dataset and its main characteristics are described in the following sections.

### 2.1.1. Geological setting and available datasets for Emilia-Romagna

The Emilia-Romagna region is located in the foreland of the south-verging central-southern Alps and the north-northeast-verging northern Apennine fold-and-thrust belts (Carminati and Doglioni, 2012), which resulted from the collision between the European and Adria plates (Figure 1). Its geographical boundaries align with the interface between the Quaternary alluvial sediments of the plain and the pre-Quaternary rocks that are exposed along the mountain fronts. The deposits include Holocene alluvial sediments, which are characterized by alternating layers of sand, silt, and clay formed in various depositional environments, such as river channels, and floodplains (Martelli et al., 2014). The alluvial sequence, dating from the Pleistocene to the Holocene, and it can be divided into two main depositional cycles: the Emiliano-Romagnolo Lower Synthem (AEI), (Middle Pleistocene), and the Emiliano-Romagnolo Upper Synthem (AES) (from Middle Pleistocene to present) (RER & ENI-Agip, 1998). This continental sequence is underlain by Lower-Middle Pleistocene deposits, primarily composed of sands with marine and transitional origins (RER & ENI-Agip, 1998). The continuous geodynamic development of the buried thrust varies in space and the temporal domain and influences the depth of the alluvial succession. In synclinal regions (e.g., the Ferrara arc), the thickness of continental deposits can exceed 500 m, while in anticlinal areas (e.g., Mirandola's ridge), it reaches approximately 100 m (RER & ENI-Agip, 1998) (Figure 1).

The northern sector of the Emilia-Romagna region belongs to the Po plain, which is the largest plain that hosts the longest watercourse of Italy (652 km) with a 74,970 km$^2$ extensive catchment (Castaldini et al., 2019). In the margin of the Apennines, a series of fluvioglacial and fluvial terraces have been observed in the old terraces unit and a system of coalescent fluvial fans developing at the Apennine foothills, related to the great amount of sediments produced during the Last Glacial Maximun (Marchetti, 2002). Furthermore, the study area includes the Adriatic sea coastline that stretches about 130 km, starting from the Po River Delta in the north and reaching the Cattolica headland in the south. The coastline of Emilia-Romagna is characterized by fluvial, transitional and marine deposits. This sandy beach includes several minor river outlets, along with numerous small harbors and large marinas scattered along its length. Additionally, there is a significant industrial port in Ravenna, which hosts facilities for the oil and chemical sectors (Ciavola et al., 2003).
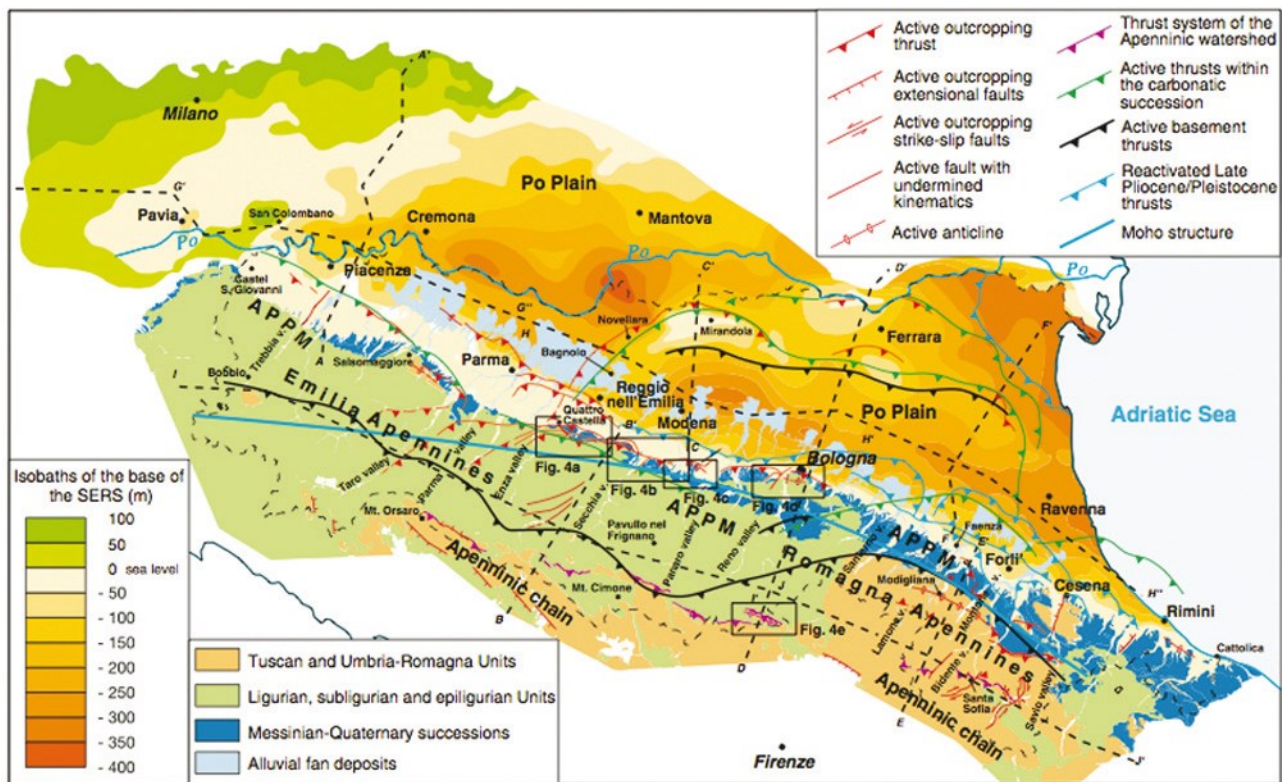
*Figure 1 – Overview of recent and active geological structures of Emilia-Romagna. Subsurface geology in the Po Plain is illustrated as isobaths of the base of the Upper Emilia-Romagna Synthem (450,000 years), APPM: Apennines–Po Plain margin. (source: Carydis et al., 2012).*

In this work, the investigated area represents the plain sector of the region, allowing for a focused study of land subsidence while excluding the southern mountain and hilly area.

The geological datasets extracted from the Emilia-Romagna region geoportal (Figure 2) include the following data:

- Geological mapping at 1:250,000, 1:50,000, 1:10,000
- Geognostic and geotechnical tests
- Geological cross-section
- Various geomorphological and anthropic elements and lines
- Structural elements
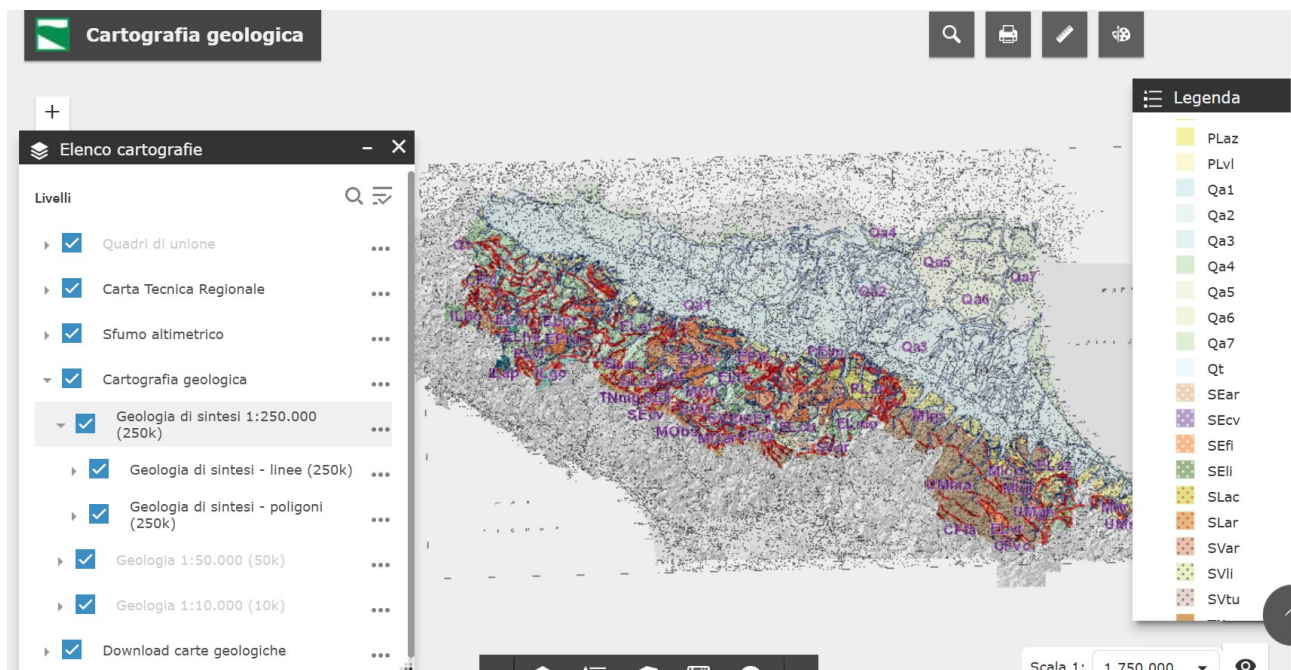- Depositional areas and lithologies
- Geological units

*Figure 2 – Overview of the Emilia-Romagna region geoportal (source: https://ambiente.regione.emilia-romagna.it/it/geologia/servizi-e-strumenti/cartografie-webgis/cartografia-geologica-1)*

The Geognostic Database was created by the Emilia-Romagna region to provide geological maps. The geological mapping at a scale of 1:50,000, as requested by the National Geological Survey under the CARG (Geological CARtography) Project derives from public and private archives, and the database is undergoing constant expansion. The Emilia-Romagna region is covered by 48 published CARG sheets with an additional 5 sheets in progress. The data can be downloaded from CARG project website (https://progetto-carg.isprambiente.it/cartografiaCARG/cartageologica.php?regione=Emilia-Romagna).

## 2.1.2. Hydrogeological setting and available dataset for Emilia-Romagna

The study area hosts a multilayer aquifer system that includes deposits originating from different regressive-transgressive cycles, consisting of alluvial cycles (aquifer groups A and B) and marine cycles (aquifer group C). Each cycle represents a hydrostratigraphic sequential unit that can be divided into other minor cycles of the A, B, and C aquifer groups, i.e. A0, A1, A2, A3, etc., where the finer sediments are at the bottom (transgressive phase) and gradually coarser sediment is at the top (regressive phase) (Figure 3). Overall, the coarse sediments, i.e., gravel, are present near the Apennine and Alpine chain in alluvial fans and at the mouth of the intramontane valleys, while the presence of medium sand and finer sediments (i.e. silt and clay) increases progressively toward the Po basin center (Amorosi et al., 1996). The deeper and confined aquifers of the alluvial plain are recharged by the rainfall input and by the hydrogeological complex of alluvial fans near the Apennines. Overall, the aquifers of the Po Plain are strongly confined vertically, but not horizontally (Marcaccio and Martinelli, 2012).
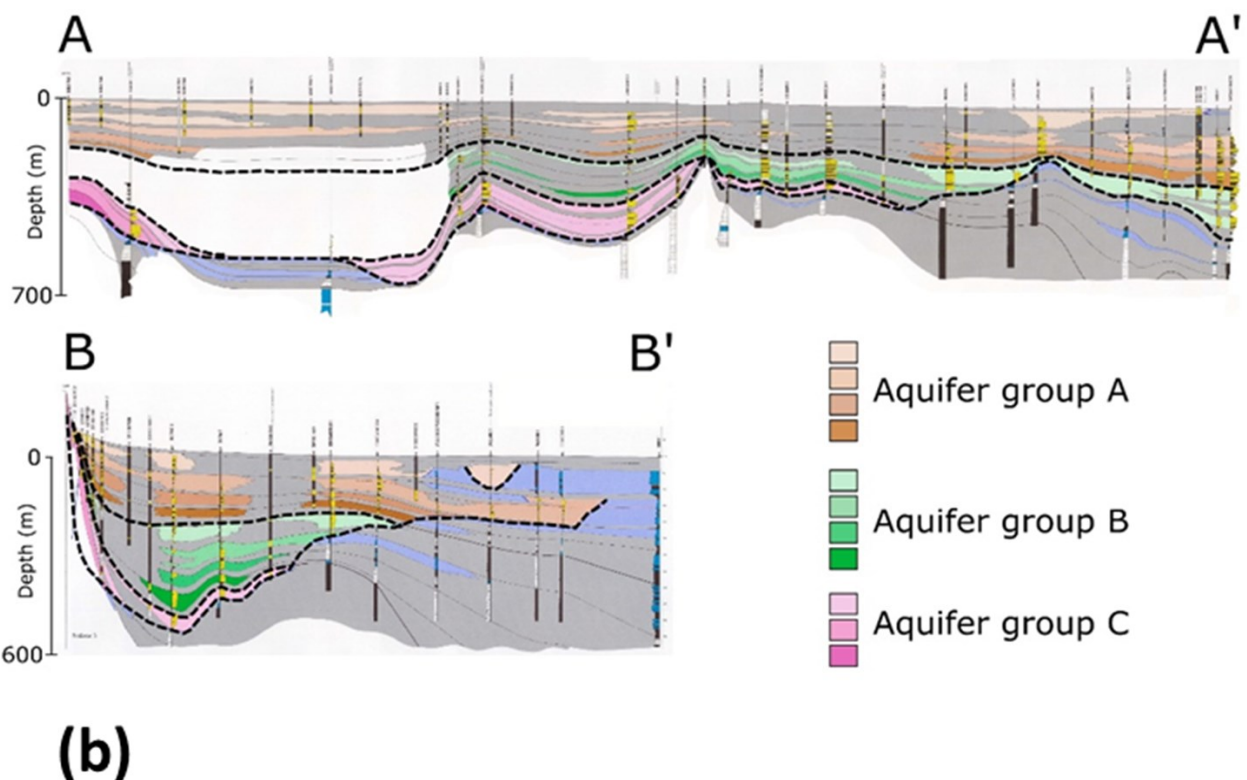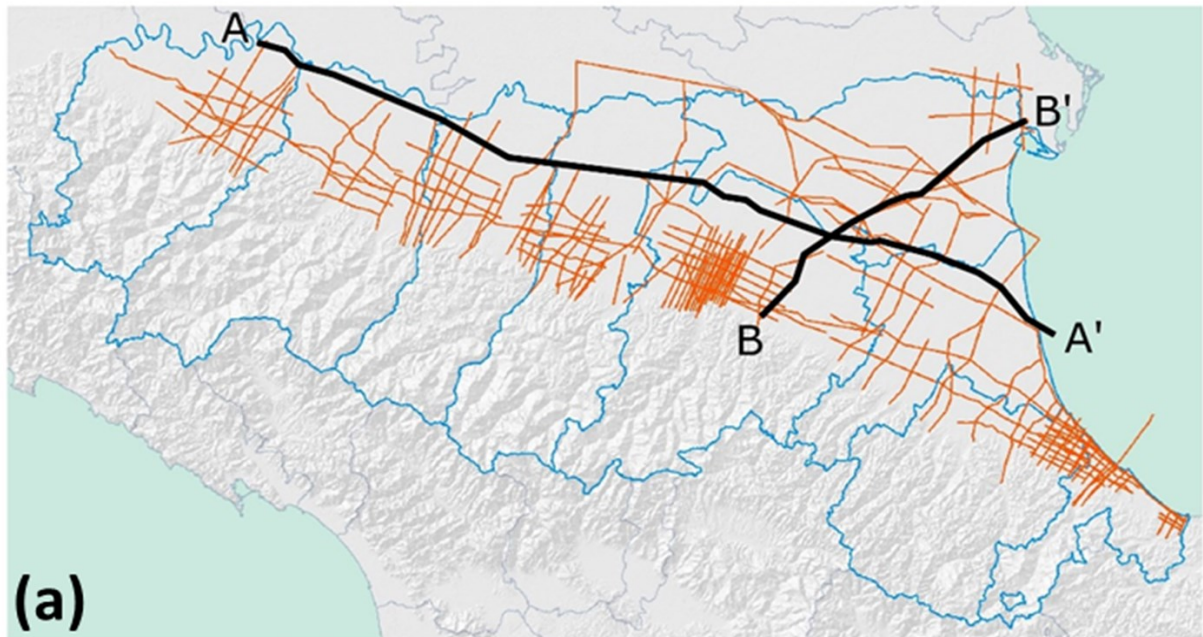
*Figure 3 – (a) Location of the hydrogeological across the study area. (b) Two representative hydrogeological cross-sections of the main aquifer groups (source: Emilia-Romagna Region, Eid et al., 2022)*

The hydrogeological datasets (Figure 4) include the following data:

- Location of qualitative-quantitative groundwater monitoring stations of the Emilia-Romagna Region

- Data on water level, expressed in meters, for each piezometric well.

The location of monitoring stations is provided in shapefile format (ETRS89/UTM-ZONE32N) and comprises information such as the ID code for each station, the elevation on the surface and the depth, and the destination of use.

Regarding the groundwater level, the data are provided as a CSV table, and the measurements are made in situ, representing the static water level expressed in meters, from which, by means of the absolute elevation above sea level of the ground level, the piezometric elevation and the sub-surface elevation are derived.
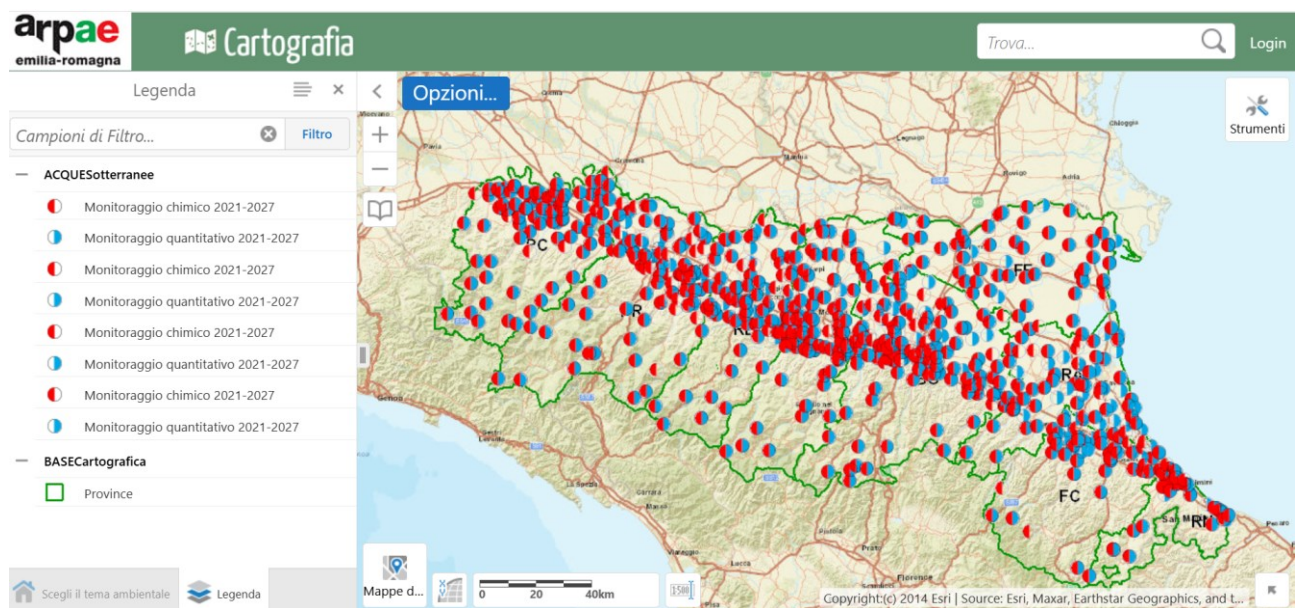


*Figure 4 – Overview of the Arpae geoportal (source: https://servizi-gis.arpae.it/Html5Viewer/index.html?locale=it-IT&viewer&viewer=Geoportal.Geoportal)*

## 2.1.3. Ground displacement observations

Satellite-derived observations of ground displacement were downloaded from the Copernicus EGMS https://land.copernicus.eu/en/products/european-ground-motion-service). The EGMS provides ground displacement based on InSAR processing of Copernicus Sentinel-1 radar imagery, updated annually and openly available to the user community (Crosetto et al., 2020). In particular, the EGMS Ortho 2018-2022 (vector) datasets were exploited for the analysis. The dataset includes displacement along the up-down (vertical) and east-west (horizontal) directions, which were derived from the combination of information provided by ascending and descending orbits of the EGMS Calibrated datasets (line-of-sight estimates, referenced to a model derived from global navigation satellite system data as described in the EGMS documentation). The available ortho datasets are resampled on a 100 m grid and distributed in raster (geotiff) and vector (comma-separated values) formats. The EGMS data include the average displacement velocity measured in mm/yr for the monitored period from 2018 to 2022 and the displacement time series in mm with a temporal sampling of 12 or 6 days following the satellite revisit time.

An overview of the dataset over the Italian territory is provided in Figure 5.
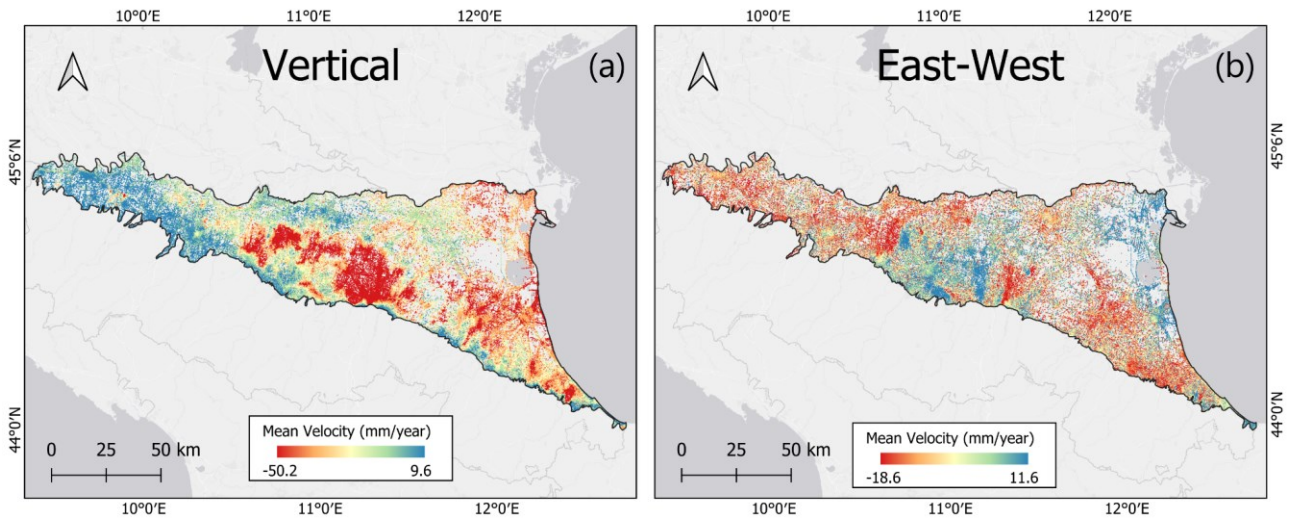
MISSIONE 4
ISTRUZIONE
RICERCA

SubRISK+

Enhancing our understanding of Subsidence RISK induced by
groundwater exploitation towards sustainable urban development

*Figure 5 – Overview of the EGMS Ortho datasets over the Emilia-Romagna region: (a) vertical, and (b) east-west displacement velocities (source: https://egms.land.copernicus.eu/).*

### 2.1.4. Urban settlement datasets

For the differential displacement risk mapping, three sources of settlement information were exploited. Specifically, two global datasets and one dataset developed and provided by the Emilia-Romagna region.

Additional details of the data are provided as follows:

(i)    The Global Human Settlement Layer (GHSL) consists of multitemporal products offering an insight into the human presence from 1975 through 2030. In particular, the Settlement Surface GHS-BUILT-S-R2023A dataset (Pesaresi et al., 2018) was derived from a composite of Copernicus Sentinel-2 2018 imagery and Landsat. The dataset depicts the distribution of built-up surfaces, expressed as square metres. The data report about the total built-up surface and the built-up surface allocated to dominant non-residential (NRES) uses. Data are spatial-temporally interpolated or extrapolated from 1975 to 2030 in 5-year intervals. For the temporal anchor point of 2018, the data is published at 10 m as observed from the S2 image data. The layer is openly available in raster format with 10 m spatial resolution, in the World Mollweide (EPSG:54009) projected system (Figure 6).
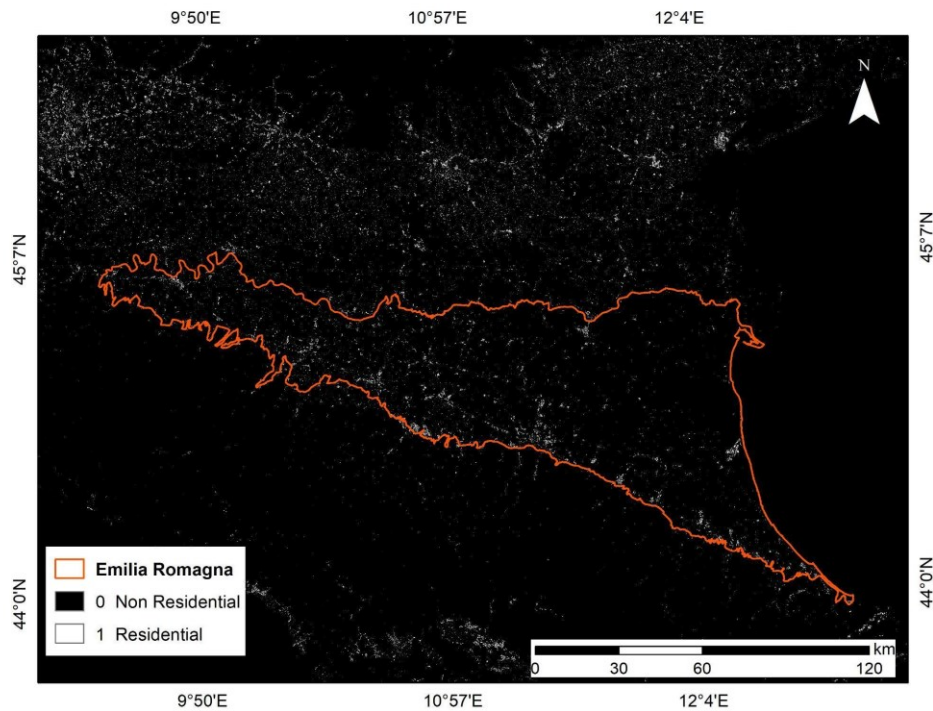
*Figure 6 – Overview of the Global Human Settlement Layer (GHSL) – GHS-BUILT-S-R2023A dataset over the Emilia-Romagna region (source:https://human-settlement.emergency.copernicus.eu/download.php?ds=bu).*

(ii)   The World Settlement Footprint (WSF®) Evolution dataset (Marconcini et al., 2021), is a 30 m resolution binary mask outlining the extent of human settlements, generated from the analysis of Landsat-5/7 data, their derived spectral indices and temporal statistics. The WSF evolution datasets are organized in 5138 GeoTIFF files (EPSG4326 projection), each one referring to a portion of 2x2 degree size (~222x222 km) on the ground. WSF evolution values range between 1985 and 2015 corresponding to the estimated year of settlement detection, whereas 0 is no data. The dataset outlines the extent of settlement (and non-settlement) areas on a yearly basis and is openly available in raster format with a reference to the WGS84 (EPSG:4326) geographic system (Figure 7).
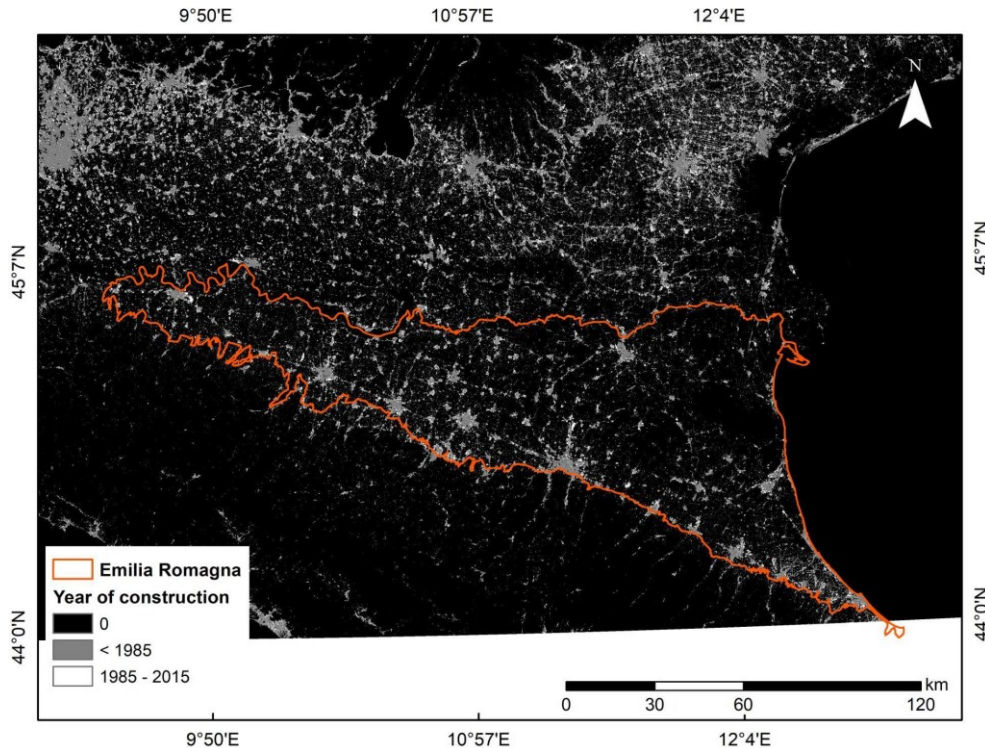
*Figure 7 – Overview of the World Settlement Footprint (WSF®) Evolution dataset over the Emilia-Romagna region (source: https://geoservice.dlr.de/web/maps/eoc:wsfevolution). The number 0 refers to no data.*

(iii)   The building footprint database (Figure 8) provided by the Emilia-Romagna region was used to extract the building area and its height. The Emilia-Romagna region, in collaboration with the Regional Agency for the Reconstruction of the 2012 Earthquake, has acquired a high-resolution orthophoto, high-resolution Digital Surface Model (DSM2018), and polygonal representation of buildings, all derived from the same aerial surveys. The polygonal layer of buildings was generated using detection techniques based on "deep learning" methodologies, with supervision and filtering of false positives and negatives, as well as integration and further refinement by specialized operators (Olivucci et al., 2019). Furthermore, through a correlation between polygonal geometries and the DSM2018 surface model, altitude attributes of elevation at the base and estimated height are associated, allowing for an estimation of the building height.

Figure 8 – Overview of the Emilia-Romagna region geoportal (source: https://geoportale.regione.emilia-romagna.it/catalogo/dati-cartografici/cartografia-di-base/xdbtr-estensione-dbtr/layer-2).

## 2.2. Methodologies

### 2.2.1. Land subsidence hotspot

The methodology to identify and map hotspots of land displacements is based on the analysis of the EGMS displacement time series. The hotspot identification uses a refinement of the method applied and tested in the Lombardy region (Righini et al., 2024). In particular, Principal Component Analysis and Independent Component Analysis (PCA-ICA) were used to identify clusters of spatial and temporal patterns of displacement. The Principal Component Analysis (PCA) is a statistical analysis used to identify a limited number of linear combinations of the original variables that account for the

greatest amount of variance among all the variables, called principal components (PCs) (Jolliffe, 1990). Independent component analysis (ICA) is a statistical approach to produce statistically independent components and not just linearly decorrelated, as with PCA. In this work, PCA was first applied to extract the number of PCs, and then ICA was used to distinguish different signals in the displacement time series, even in the case of spatial correlation (Gaddes et al. 2018). The procedure allows for obtaining, for each measuring point (MP), the score of the independent components (ICs), which indicates the degree of correlation with the main detected trends.

Then, the database of the land subsidence hotspots (LH) is created by applying the optimized hot spot analysis (OHSA) to find clusters of MPs with similar trends. This spatial statistic tool allows us to detect high and low values of IC scores based on the Getis-Ord Gi* statistic (Ord et al., 1995). The significant hotspots are identified using a 90% confidence level, and successively, the preliminary results are filtered by considering clusters with at least five MPs and an extension higher than 5000 $m^2$.

## 2.2.2. Drivers of the land subsidence hotspots

Land subsidence in the plain portion of the Emilia-Romagna region is widely documented since the past century (Carbognin et al., 1984, Gambolati et al., 1991, 1999, Bitelli et al., 2000, Teatini et al., 1998, Baldi et al., 2009, Nespoli et al., 2021) and monitored by ARPAE (https://www.arpae.it/it/temi-ambientali/suolo/subsidenza). In particular, previous authors have recognised natural causes of land subsidence due to compaction of recent alluvial soils and tectonic movements (Amorosi et al., 1999, Carminati and Martinelli, 2002, Bruno et al., 2020) and anthropogenic factors such as the extraction of groundwater from confined or semi-confined deep aquifers (Teatini et al., 2006) and hydrocarbon production and post-production (Gambolati et al., 1998, Teatini et al., 1998, Baú et al., 2000, Taramelli et al. 2015, Fiaschi et al., 2017).

In this work, to understand the drivers of the land subsidence, the LH database has been cross-compared with different ancillary data such as geological, hydrogeological data, CORINE Land Cover Change, provided by the Copernicus Land Monitoring Service, hydrocarbon storage and production sites. The investigation is performed to find cause-effect relationships between the different variables at a local scale (Bonì et al., 2016).

## 2.2.3. Differential displacement risk mapping

The differential displacement risk mapping over the Emilia-Romagna region is assessed by applying a refinement of the methodology developed at the national scale in the SubRISK+ project (Cigna et al., 2024). In this approach, the level of risk is provided for each building. The differential displacement risk level is related to the combination of the hazard and exposure-vulnerability classes using a risk-matrix approach.

The hazard levels induced by differential displacement on urban infrastructures can be estimated through the computation of the angular distortion ($\beta$) (Skempton & McDonalds, 1956) and horizontal strain ($\varepsilon$) (Tandanand & Powell, 1991), as derived from the EGMS satellite InSAR datasets (see section 2.1.3). These two parameters are widely exploited in geotechnical engineering (Burland and Worth, 1974) and are among the main subsidence-related intensity parameters determining the building damage severity, together with construction year, type, characteristics and maintenance state of the superstructures and their foundations (Peduto et al., 2017).

The computation of these two parameters starts by accounting for the vertical ($V_U$) and east-west ($V_E$) displacement velocity data provided by the EGMS Ortho layers for the 2018-2022 period (Figure 6a-b). Considering that the Emilia-Romagna region has been historically affected by land subsidence since the 1950s (Caputo et al., 1970; Bitelli et al., 2000; Teatini et al., 2006), the total cumulated angular distortion and strain are estimated using a 30-year period. This assumption implies that the detected average velocity for the period 2018-2022 is assumed to be constant for the last 30 years. Similar considerations are available in the literature (Barra et al., 2022). It is worth noting that locally, some accelerations or decelerations of the trend can occur, but we assume that the chosen scenario to evaluate the expected angular distortion and strain is plausible for the risk analysis.

The total displacement values along the vertical and east-west directions, $d_U$ and $d_E$ respectively, and the total angular distortion and horizontal strain, $\beta$ and $\varepsilon$ (Figure 6c-d), are calculated at each pixel as follows:

Total vertical displacement $\quad d_U = V_U*30$ $\qquad$ Total east-west displacement $\quad d_E = V_E*30$

Total angular distortion $\quad \beta = \dfrac{d_{U_j} - d_{U_i}}{l}$ $\qquad$ Total horizontal strain $\quad \varepsilon = \dfrac{d_{E_j} - d_{E_i}}{l}$

where $d_{Uj}$ and $d_{Ui}$ are the vertical (and east-west) displacements of adjacent measuring points $j$ and $i$, and $l$ is their planar distance (in this case, this equals the spatial resolution of the EGMS Ortho datasets, i.e. 100 m). Whereas $d_{Ej}$ and $d_{Ei}$ are the east-west displacements of adjacent measuring points.

Hazard levels are identified according to a scale ranging from low (H1) to very high (H4) (Figure 9e), indicating an increasing possibility of the occurrence of fissuring/fracturing and associated damage to buildings. The threshold values adopted for $\beta$ and $\varepsilon$ account for geotechnical practice (CEN *Eurocode 7, 2004*) and past InSAR-based structural health applications (Cigna & Tapete, 2021-a; Cigna & Tapete, 2021-b; Cigna & Tapete, 2022; Sanabria et al., 2014; Qu et al., 2014; Zho et al., 2018). With regard to $\beta$, the thresholds adopted to classify the angular distortion are: 1/3000 (equivalent to 0.033%), 1/500 (0.2%), and 1/150 (0.667%). As for $\varepsilon$, the threshold adopted to categorize the strain is: ±0.03% (namely 0.03%, applied to the absolute value of the strain, independently of its direction).

Then, hazard scores based on $\beta$ are geospatially complemented with information on the presence/absence of significant $\varepsilon$ that potentially could also threaten the structures (Figure 9e): an increase in the hazard score obtained by classifying $\beta$ is considered whenever the value of $\varepsilon$ exceeds the adopted threshold. The hazard level is finally mapped across the Emilia-Romagna region, at the 100 m spatial resolution provided by the EGMS Ortho datasets (Figure 9f).

The table in panel (e):

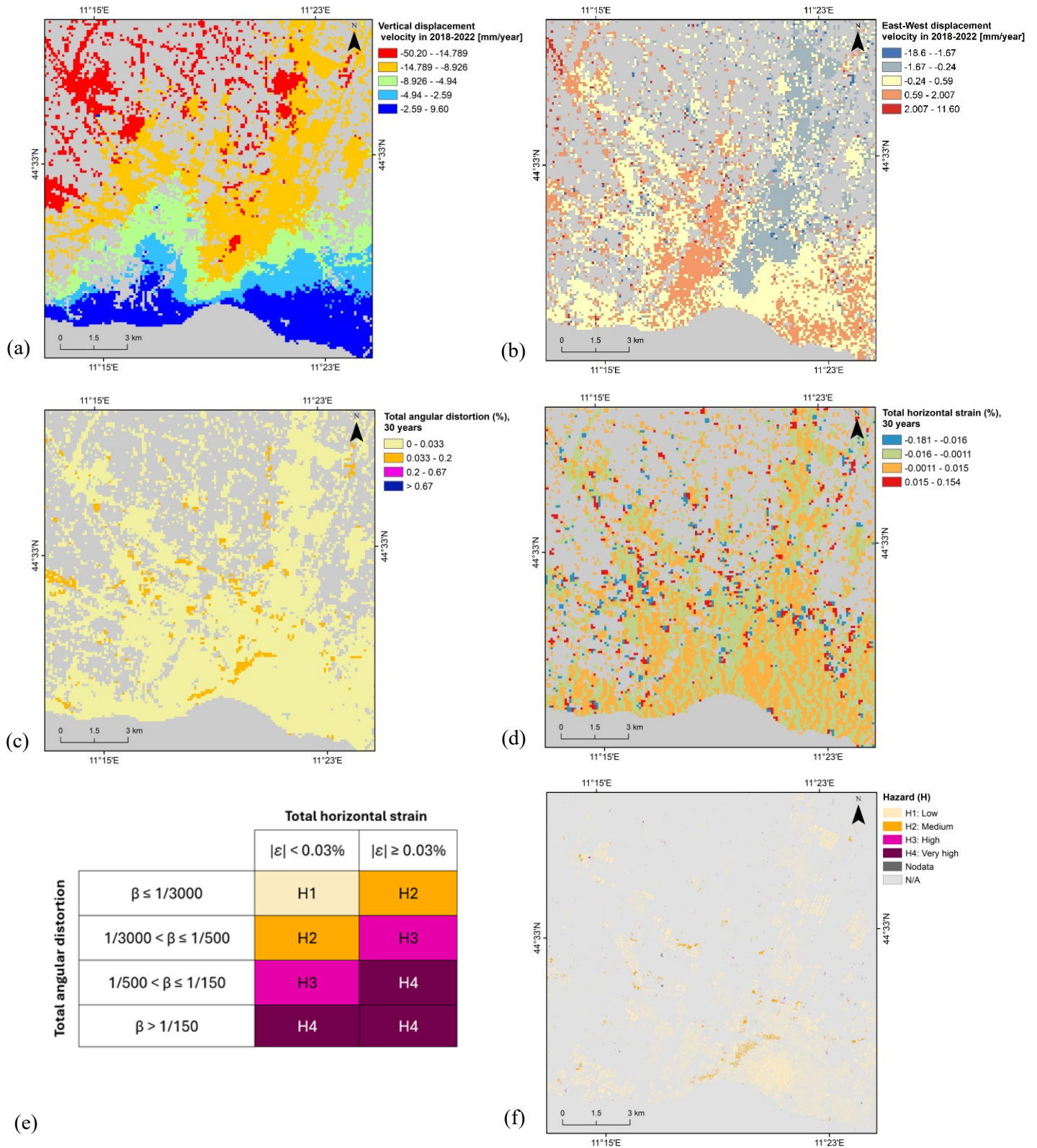| | Total horizontal strain | |
|---|---|---|
| **Total angular distortion** | $|\varepsilon| < 0.03\%$ | $|\varepsilon| \geq 0.03\%$ |
| $\beta \leq 1/3000$ | H1 | H2 |
| $1/3000 < \beta \leq 1/500$ | H2 | H3 |
| $1/500 < \beta \leq 1/150$ | H3 | H4 |
| $\beta > 1/150$ | H4 | H4 |

*Figure 9 – Example of Hazard (H) assessment and mapping using SubRISK+ methodology: (a) EGMS Ortho vertical and (b) EGMS Ortho east-west displacement velocity datasets, (c) total angular distortion and (d) horizontal strain over a period of 30 years, (e) H level assessment approach, and (f) resulting H map.*

Exposure and vulnerability of urban infrastructure are assessed based on its spatial distribution, type, height, and year of construction. Data on the type (residential, non-residential), height (≤ 3 m, 3-6 m, 6-15 m, 15-30 m, or > 30 m) and age (pre-/post-1985) of built-up surfaces are derived from the three urban settlement datasets (see section 2.1.4): building upon type of buildings extracted from the GHS-BUILT-S settlement surface (Figure 10a), then complementing with information on building age as derived from the WSF Evolution layer (Figure 10b), and height of building extracted from Emilia-Romagna region database.

A combined Exposure-Vulnerability (EV) metric is therefore established based on the integration of GHS-BUILT-S and WSF Evolution data (Figure 10c), with values ranging between low (EV1) and very high (EV4). The metric assumes increasing levels of potential damage that could affect the buildings exposed to the hazard, when moving from lower to taller buildings, from non-residential to residential structures (the latter are assumed more likely to have loose foundations), and newer to older constructions (the latter are potentially more vulnerable with respect to new constructions complying with recent structural engineering regulations; CEN Eurocode 7, 2004). Following the geospatial integration of the two layers, the EV metric is then spatially mapped across the Emilia-Romagna region buildings (Figure 10d).



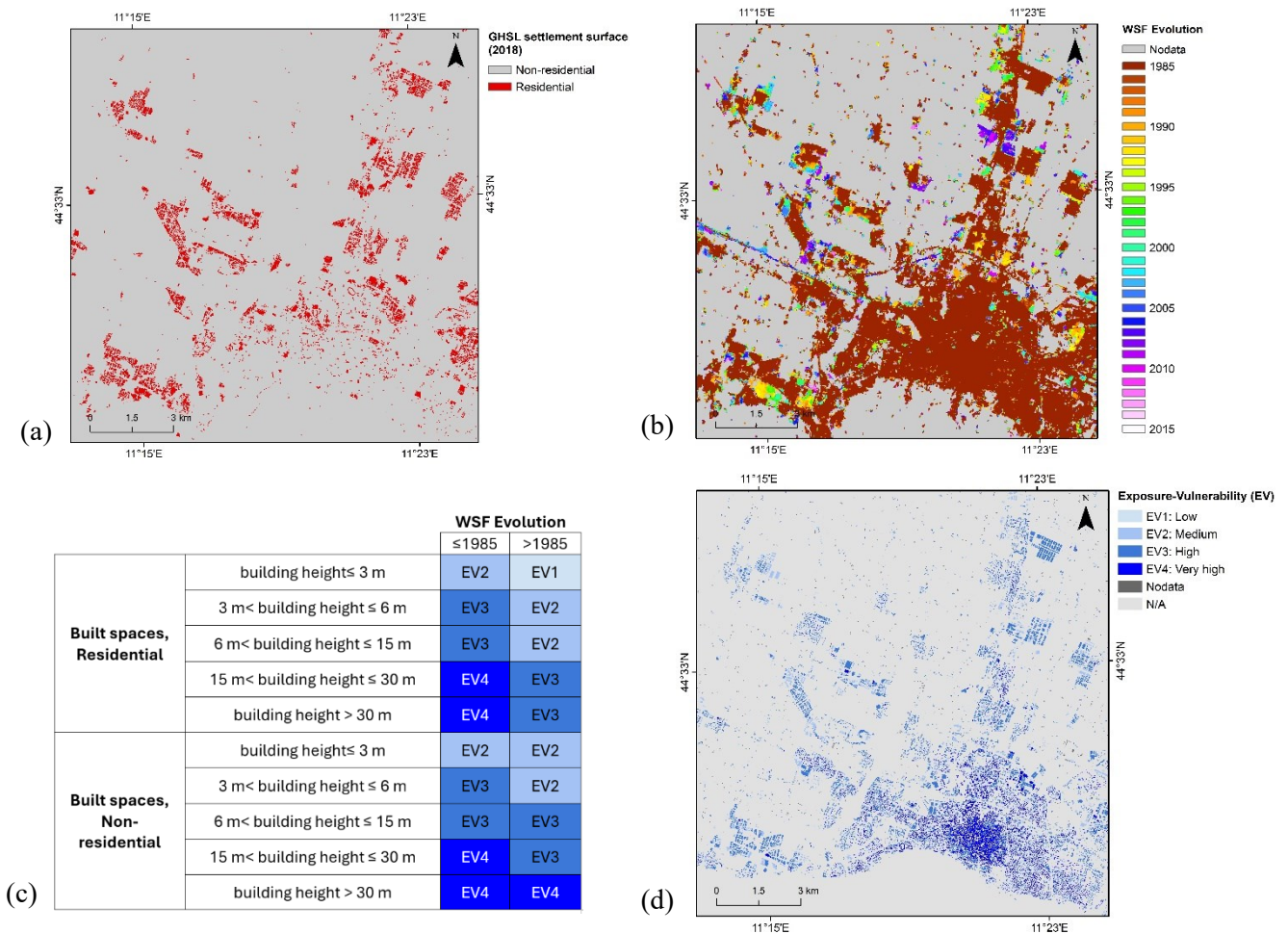|  | | WSF Evolution | |
|---|---|---|---|
|  | | ≤1985 | >1985 |
| **Built spaces, Residential** | building height ≤ 3 m | EV2 | EV1 |
|  | 3 m < building height ≤ 6 m | EV3 | EV2 |
|  | 6 m < building height ≤ 15 m | EV3 | EV2 |
|  | 15 m < building height ≤ 30 m | EV4 | EV3 |
|  | building height > 30 m | EV4 | EV3 |
| **Built spaces, Non-residential** | building height ≤ 3 m | EV2 | EV2 |
|  | 3 m < building height ≤ 6 m | EV3 | EV2 |
|  | 6 m < building height ≤ 15 m | EV3 | EV3 |
|  | 15 m < building height ≤ 30 m | EV4 | EV3 |
|  | building height > 30 m | EV4 | EV4 |

*Figure 10 – Example of Exposure-Vulnerability (EV) assessment and mapping using SubRISK+ methodology: (a) GHSL Settlement Characteristics, (b) WSF Evolution, (c) EV metric assessment approach, and (d) resulting EV map.*

Hazard and exposure-vulnerability information are finally integrated via the implementation of a tailored risk matrix, enabling the classification of risk levels into (Figure 11a):

| Low (R1) | This is considered a low risk level. |
|---|---|
| Medium (R2) | This is a medium risk level, large-scale satellite monitoring is recommended. |
| High (R3) | This is a relevant risk level, suggesting that potential structural damage might occur at the urban infrastructure involved; therefore, field surveys should be performed to validate these findings. |
| Very high (R4) | This is the highest risk level, indicating a high likelihood of occurred/incipient structural damage; field surveys should be performed to validate these findings. |

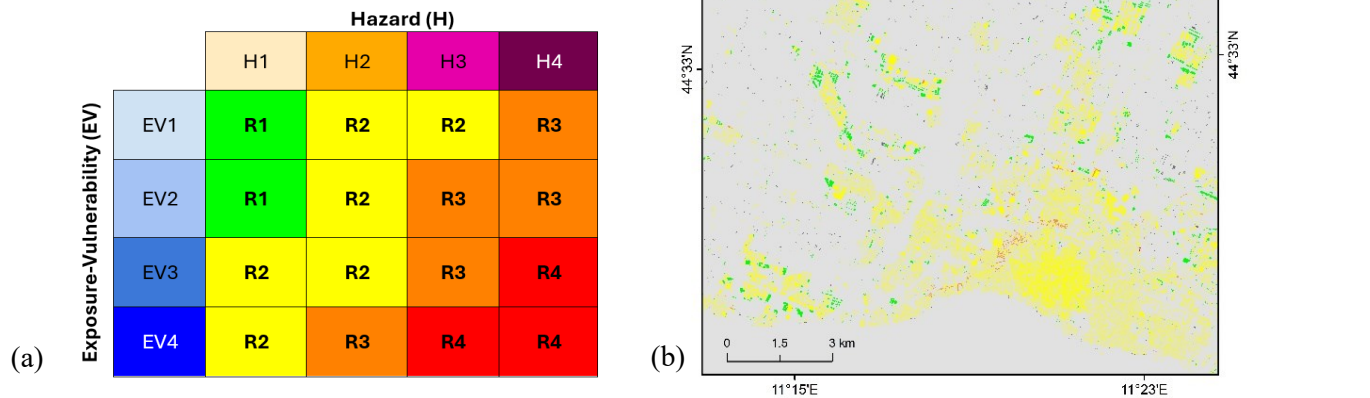An example of the resulting risk map is provided in Figure 11b.



*Figure 11 – Example of Risk (R) assessment and mapping using SubRISK+ methodology: (a) risk matrix, and (b) resulting risk levels mapping.*

# 3. RESULTS

## 3.1.    Land subsidence hotspot in the Emilia-Romagna region

The PCA analysis of the vertical displacement time series gives insight into three main components. Indeed, the PC1 explains 94% of the variance, and PC2 and PC3 explain, respectively, 1% and 0.5% of the variance (Figure 12).


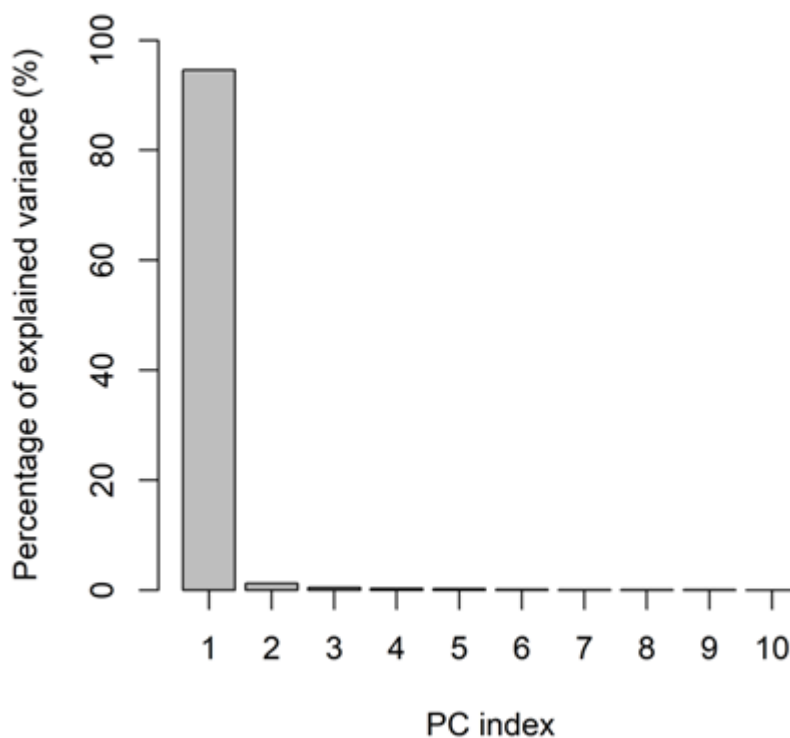
*Figure 12 – Percentage of explained variance of the vertical ground deformation.*

The visual inspection of the independent components' eigenvectors shows that the first component (IC1) corresponds to the long-term linear trend. The second one (IC2) corresponds to a long-term non-linear trend with a short-term seasonal component, and the third IC highlights seasonal displacements (Figure 13).
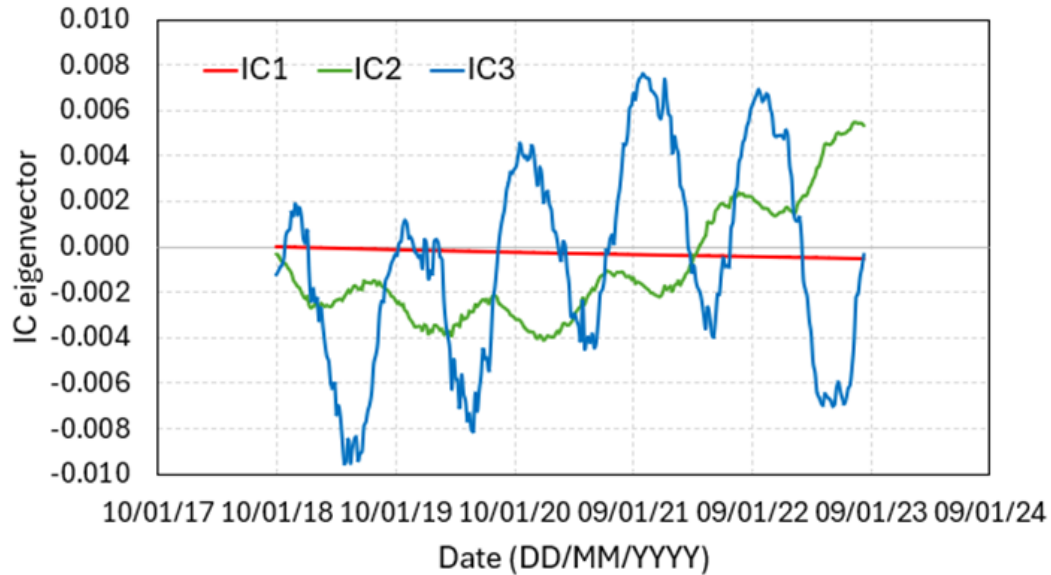
*Figure 13 – IC eigenvector value of the three components of the EGMS dataset.*

Figures 14, 15, and 16 show the spatial distribution of the independent component scores of the IC1, IC2, and IC3, respectively. The spatial pattern of the IC1 of the displacement highlights that the component is mainly located in the Bologna and Reggio Emilia provinces. The IC2 is mainly localized in proximity to the Apennine alluvial fans. Finally, the IC3 is mainly located in Ravenna province.
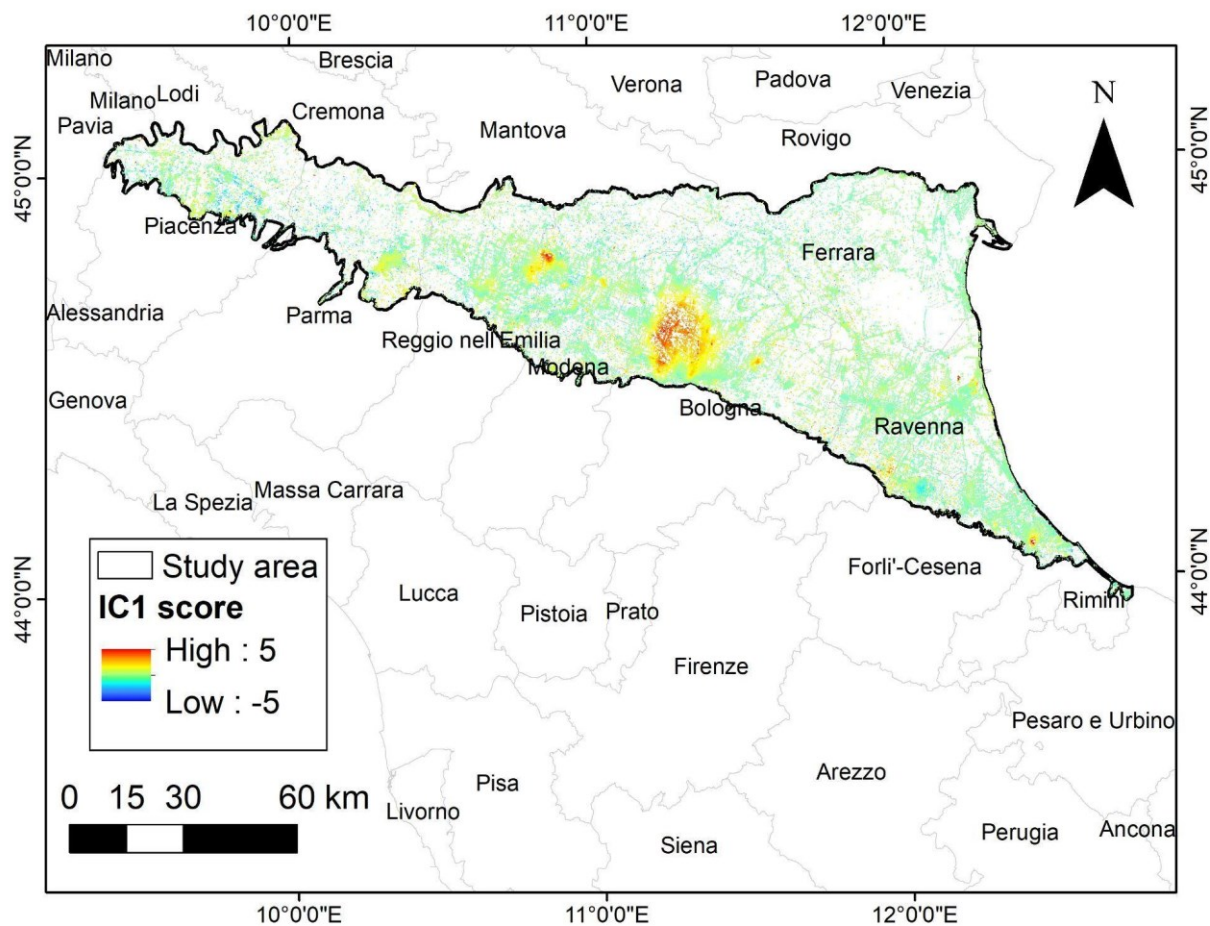
*Figure 14 – IC1 score maps over the plain area of the Emilia-Romagna region. The name of the Italian provinces is also reported.*
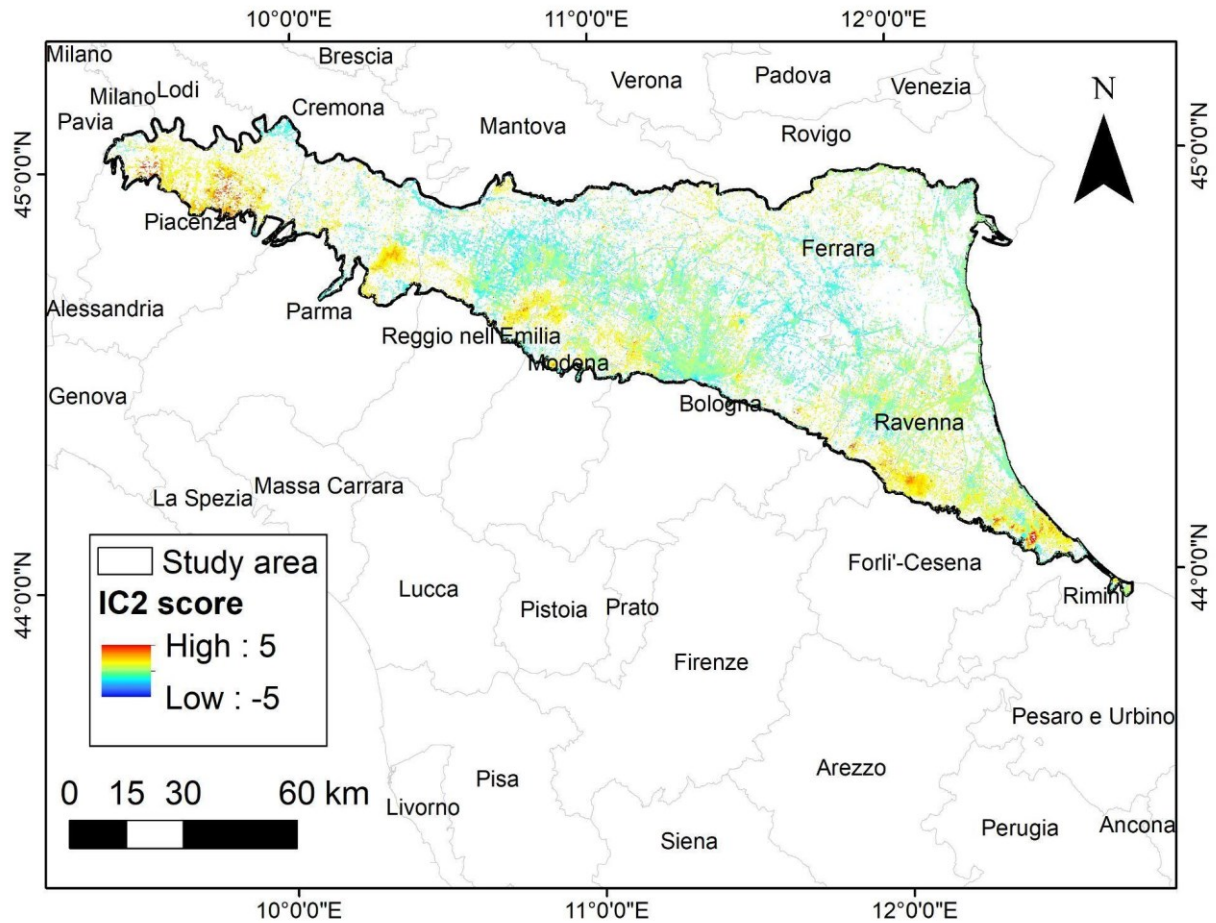
*Figure 15 – IC2 score maps over the plain area of the Emilia-Romagna region. The name of the Italian provinces is also reported.*
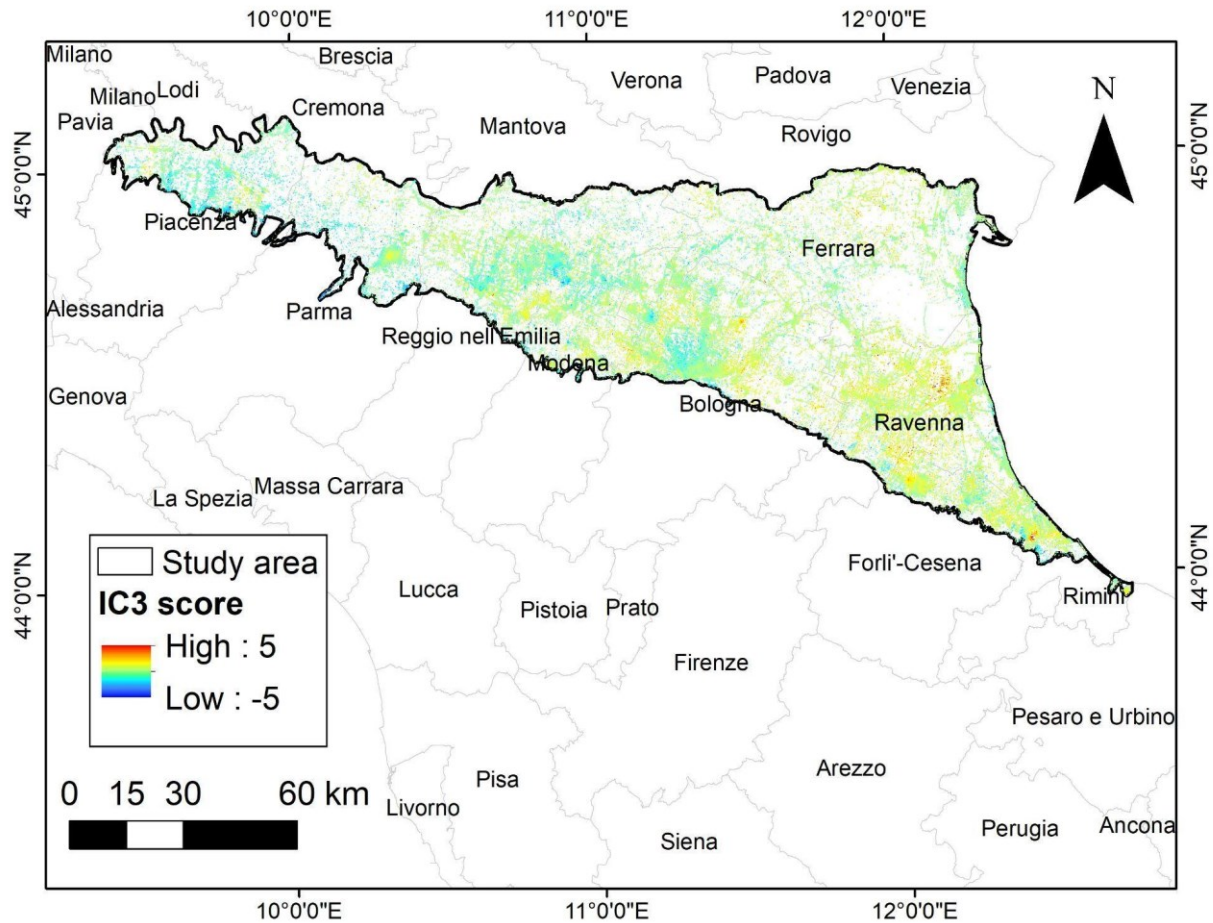
*Figure 16 – IC3 score maps over the plain area of the Emilia-Romagna region. The name of the Italian provinces is also reported.*

Land subsidence hotspots (LH) have been delineated using the approach described in section 2.2.

The results show that 17.5% of the LH are detected using IC1, while 44.9% and 37.6%, using IC2 and IC3, respectively (Figure 17). In terms of area coverage, the LH IC1 encompasses a total area of about 300 km$^2$, while LH IC2 and LH IC3 encompass about 400 km$^2$ each. In terms of minimum vertical velocity detected in the LH, the average value in the LH IC1 is -7.5±1.1 mm/yr. Regarding the LH IC2 and LH IC3, the values reach -1.4±0.8 mm/yr and -3.6±0.9 mm/yr, respectively.

*Figure 17 – LH of the three independent components over the plain area of the Emilia-Romagna region. The name of the Italian provinces is also reported.*

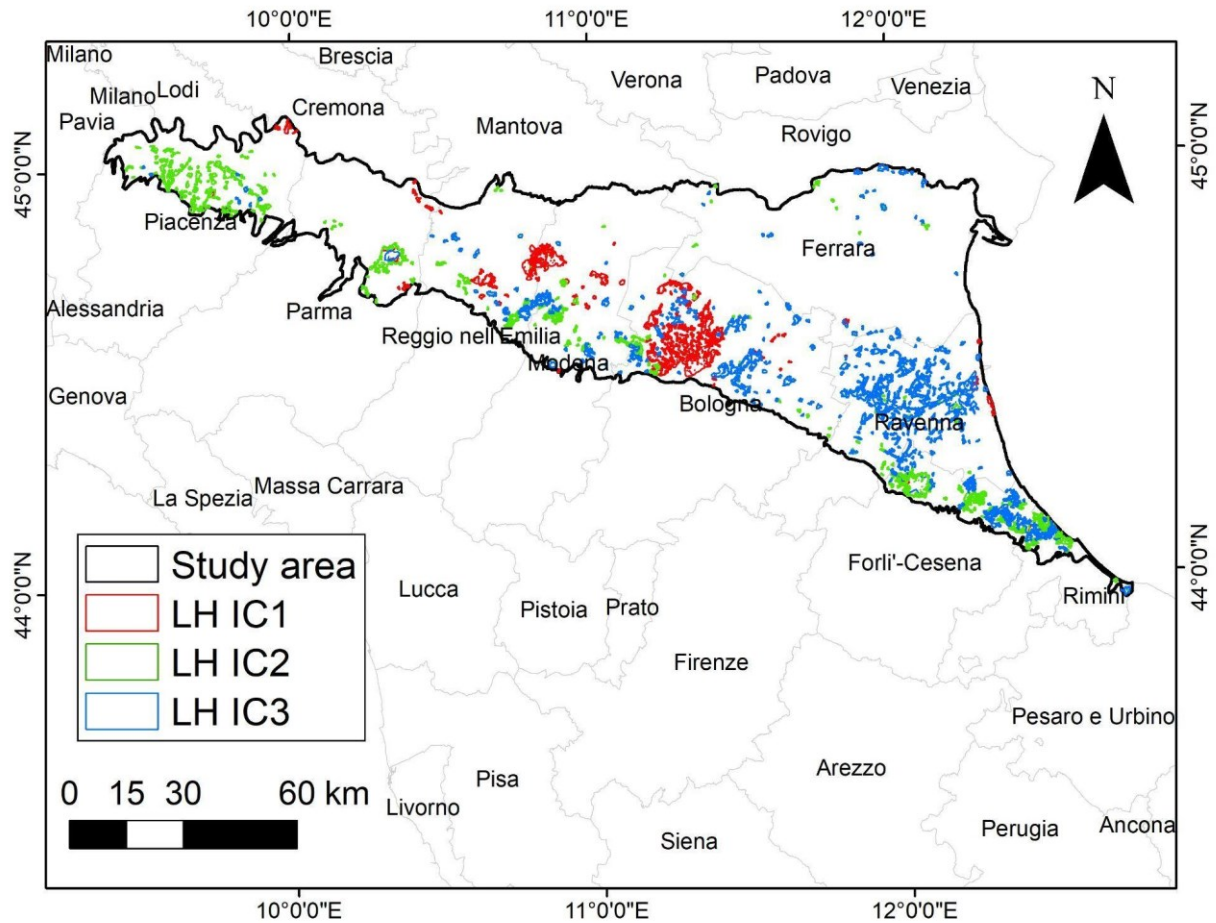The LH IC1 is mainly observed in Bologna province, while the LH IC2 zones are observed in Forlì-Cesena and Piacenza. The LH IC3 zones are observed in Ravenna province (Figure 18).
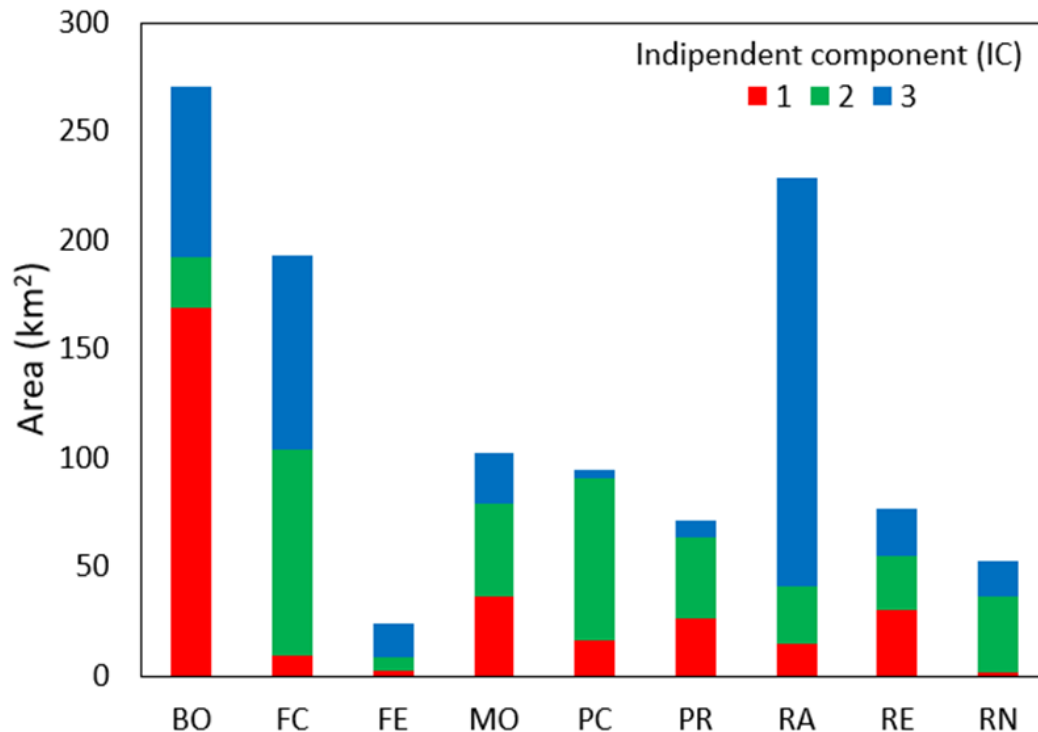
*Figure 18 – Area of the LH of the three independent components in the Emilia-Romagna provinces. "BO" stand for Bologna, "FC" is Forlì-Cesena, "FE" is Ferrara, "MO" is Modena, "PC" is Piacenza, "PR" is Parma, "RA" is Ravenna, "RE" is Reggio Emilia, and "RN" is Rimini.*

## 3.2.     Natural and anthropogenic drivers of land subsidence

A spatio-temporal analysis is performed to interpret various drivers of the detected land subsidence. The selected variables are chosen taking into account the previous authors' evidence, as described in section 2.2.2.

### 3.2.1. Tectonic control on the land subsidence

In the area of Carpi-Correggio, an extensive LH IC1 of about 18.85 km$^2$ is evident (Figure 19). This land subsidence hotspot is characterized by an average vertical velocity of -10.0 mm/yr and a maximum rate of -25.0 mm/yr in the period 2018-2022. In particular, these movements are detected in proximity to the Campegine-Correggio seismogenic sources. This composite source is located to the northeast of Reggio Emilia and is part of the Ferrara Arc thrust front. This fault system represents the NW- to N-verging external arc at the northeastern edge of the Northern Apennines chain (Boccaletti et al., 2011). The vertical and east-west velocity profiles show ground displacement changes aligned with the buried geological structures. Furthermore, in this area, groundwater level changes are not evident. Therefore, these evidences suggest that the detected displacements are most likely related to the tectonic activity of these geological structures.
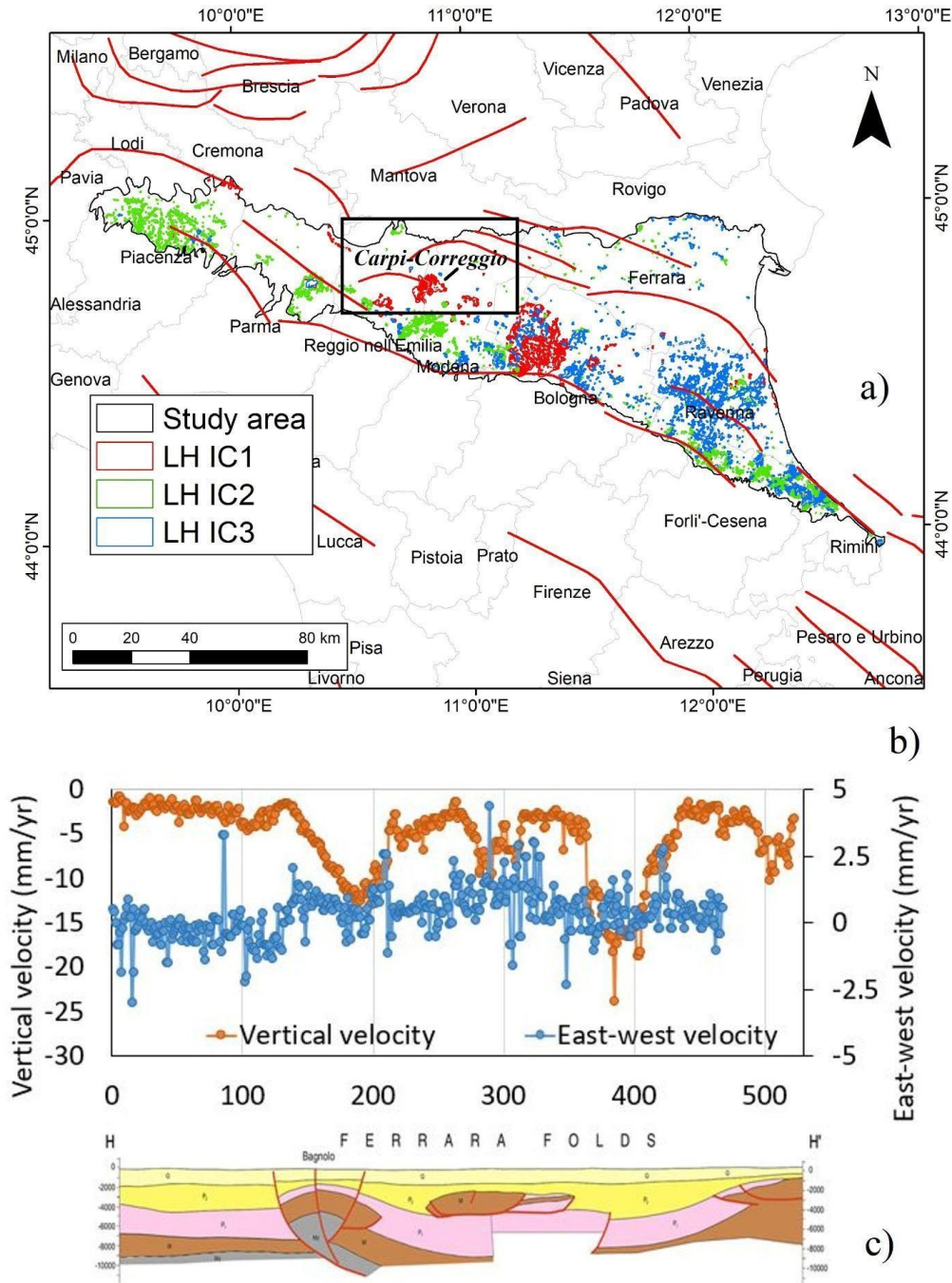
*Figure 19 – a) Location of the LH IC1, LH IC2 and LH IC3 and faults represented as red lines. Source: DISS Working Group. (2025). b) Vertical and East-west velocity profiles and c) geological cross-section. Source. Boccaletti et al. 2011. See the geological cross-section location in Figure 1.*

### 3.2.2. Land movements and shallow geology

To investigate the role of shallow geology (about 30-100 m in depth), we extracted data about the depositional environments and lithological classes from the geological dataset of the Emilia-Romagna region (Figure 20a). As previously mentioned in section 2.1.1., the CARG dataset is not available for the northern zone of the study area.

The study area has been subdivided into three main depositional environments: the alluvial plain, the coastal plain, and the deltaic region of the Po River plain. For the lithological classes, the simplified classes are listed below:

-clay; this class includes clay, silty clay, silt, silty clay

-sandy clay; this class includes sandy clay, sandy silts, sandy clayey silt

-gravel, sand; this class includes gravel, sand, sandy gravel

-clayey gravel: this class includes clayey gravel, clayey-sandy gravel

-silty clay with peat: this class includes silty clay with peat.

The results indicate that the highest value of the average land subsidence rates occurs in the clayey deposits of the coastal plain, reaching a value of -6.8 mm/yr (Figure 20). This phenomenon may be influenced by the compaction of recent soft soils in the study area, but the role of deeper causes cannot be excluded in this analysis. Indeed, the tectonic activity also plays a role in the thickness of the compressible soils (Cigna et al., 2012).
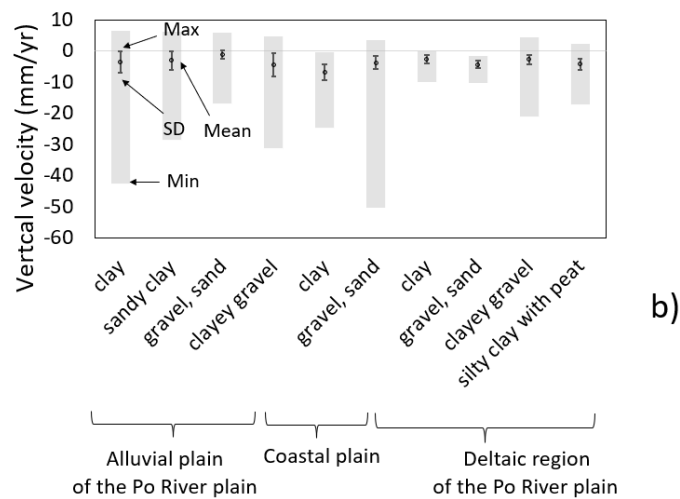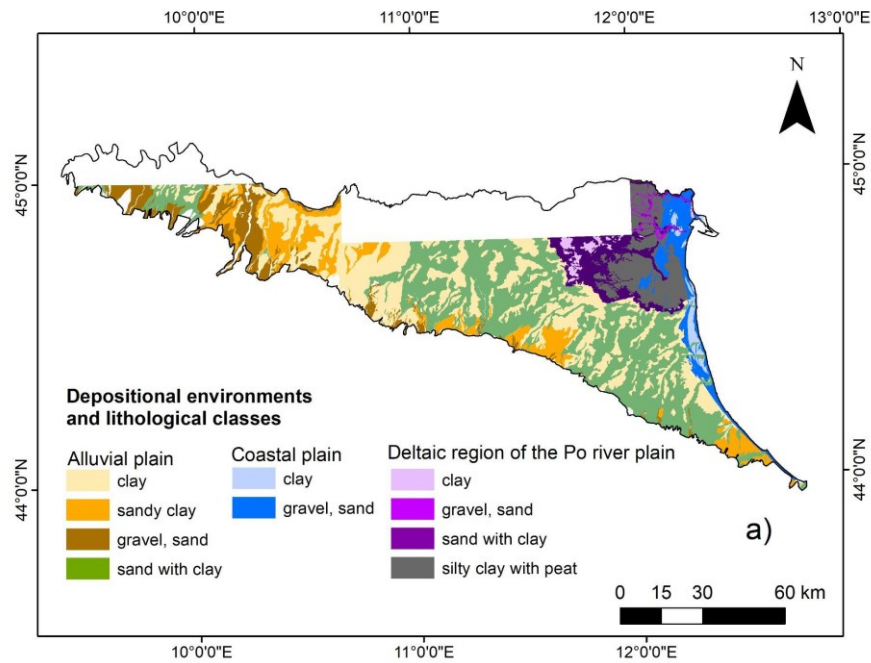
In the three depositional contexts, the minimum vertical velocity values are observed in different lithological classes. In the alluvial plain, the highest minimum velocity is observed in clayey deposits, while in the coastal plain, it is found in gravel and sand deposits. In the delta area, the highest minimum velocity is associated with sand mixed with clay deposits. Notably, we also observed minimum velocity rates of -20.0 mm/yr in silty clay deposits containing peat, which could be attributed to peat oxidation in these deltaic soils.

When considering the different ICs, the LH ICs are predominantly found in the alluvial plain, particularly in regions with sand and clay deposits. It is worth noting that the area of the alluvial plain is much larger than that of the other two environments. Furthermore, additional phenomena are reported for these areas such as the groundwater extraction of the multi-layer aquifer systems of the alluvial plain.

Specifically, LH IC1, IC2, and IC3 collectively cover an area of over 200 km² within this lithological class. The most extensive LH ICs correspond to the third component, which is associated with seasonal deformation. These seasonal deformations may be linked to the seasonal compaction of aquifers in the alluvial plain. In the alluvial plain, the largest areas of deformation for clay and sandy clay deposits are attributed to LH IC1, while for gravel and sand lithological classes, the most extensive areas belong to LH IC2 (Figure 20c).

In both the coastal plain and delta deposits, we observed that LH IC3 areas exhibit higher values compared to LH IC1 and LH IC2. This evidence seems to be due to the broader scale of the third component compared to the localized hot spots represented by LH IC1 and LH IC2. Consequently, in these depositional environments, the LH IC1 and LH IC2 drivers may be attributed to local anthropogenic effects.

Further localized analyses have been conducted to explore the correlation between seasonal and long-term groundwater levels and changes in ground deformation, with findings detailed in the subsequent paragraphs.

MISSIONE 4
ISTRUZIONE
RICERCA

SubRISK+
Enhancing our understanding of Subsidence RISK induced by
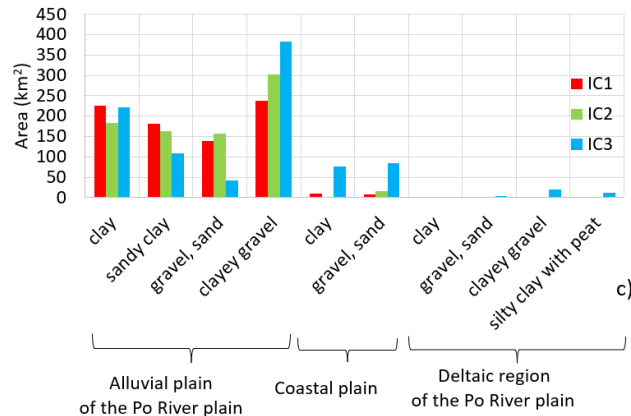groundwater exploitation towards sustainable urban development

*Figure 20 – a) Simplified depositional environments and lithological classes of the study area. b) Box-plot of the statistical parameters for each lithological class in the three depositional environments. c) Area (km²) of LH detected by IC1, IC2, and IC3 for each lithological class in the three depositional environments.*

### 3.2.3. Hydrogeological control on the land subsidence

To conduct the investigation of the hydrogeological control on the land subsidence, we selected the ARPAE monitoring stations (piezometers) of the upper and lower confined aquifers (Aquifer group A-C) and the LH with at least one monitoring station. The results show that 4% of the detected ground displacement hotspots include at least one piezometer. The selected piezometers allow us to monitor various groundwater bodies of the Emilia-Romagna region (Figure 21a).

Then, for each piezometer, the groundwater level and ground displacement changes have been estimated over the period 2018-2022. The results give preliminary insight into the different relationships between the groundwater level variations and ground movements. Indeed, high values of about 5 m of groundwater level decline (i.e., negative groundwater level changes) are observed for the lower confined layers of the Reno-Lavino alluvial fan located in proximity to Bologna, which corresponds to values greater than -40 mm of land displacements. A high variability is evident for the piezometers of the lower confined layers of the Po River floodplain. For these monitoring stations, even a decline in groundwater level lower than 2 m corresponds to a land displacement higher than -20 mm (Figure 21b). In these cases, additional factors (for example, a more compressible or thicker depleted aquifer, rather than different processes) should be accounted for to justify these movements.

The piezometers of the Reno-Lavino alluvial fan are included in LH IC1, whereas the piezometers of the lower confined layers of the Po river floodplain and the alluvial fans are mainly located within LH IC2 and LH IC3. Therefore, especially for the LH IC3, additional investigations are necessary to explain the seasonal movements as described in the following paragraph 3.2.3.

It is worth noting that in this analysis, the possible delayed cause-and-effect relationship between pressure decline and land subsidence are not taken into account. Local-scale physics-based investigations of the hydrogeological setting and pore pressure distribution should be conducted to further consider this issue. Furthermore, the interpretation cause-and-effect relationship could be improved by future Earth Observation (EO) products, such as those offered by the IRIDE program. In particular, the IRIDE constellation is a programme financed in the framework of the European Union—Next Generation EU (PNRR-M4C2) Italian National Recovery and Resilience Plan (PNRR).

MISSIONE 4
ISTRUZIONE
RICERCA

SubRISK+

Enhancing our understanding of Subsidence RISK induced by
groundwater exploitation towards sustainable urban development

IRIDE will offer sixty-nine satellites and eight macro-services, which will include two SAR constellations in Band-X with an improved product latency and the possibility to measure the North-South deformation component (Conti et al., 2024, Cotugno et al. 2024).
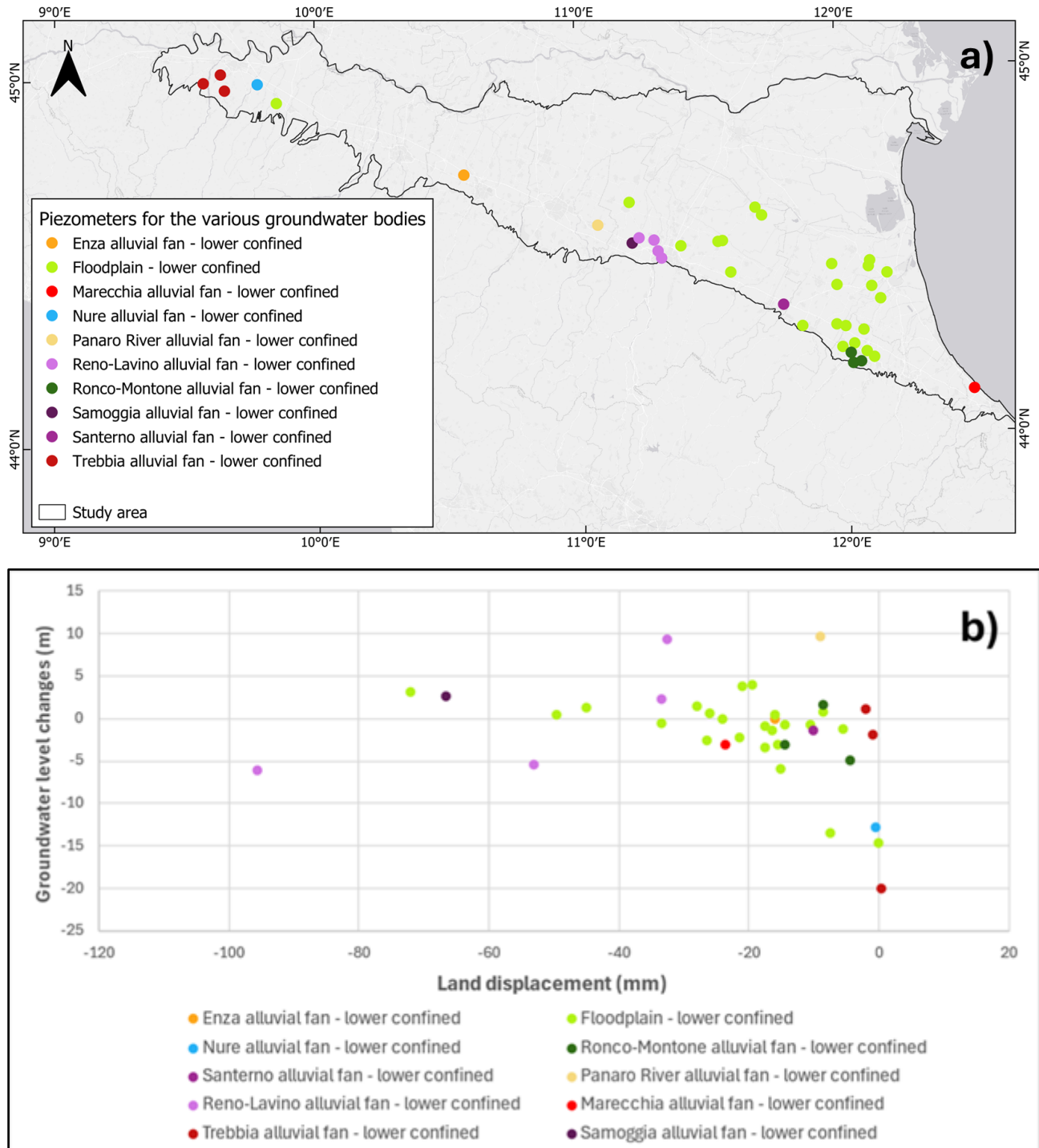


*Figure 21 – (a-g) Location of the selected ARPAE piezometers within the LH database for the various groundwater bodies of the Emilia-Romagna region. Cross-comparison between the groundwater level changes and the land displacements for various groundwater bodies over the period 2018-2022.*

MISSIONE 4
ISTRUZIONE
RICERCA

SubRISK+

Enhancing our understanding of Subsidence RISK induced by
groundwater exploitation towards sustainable urban development

### 3.2.4. Role of the seasonal hydrological changes

In the Ravenna province, an area exceeding 67 km² is characterized by LH IC3, i.e. primarily by seasonal ground displacements (Figure 22a). In this area, the shallow deposits, extending to a depth of 30 meters, include thick layers of soft silty clay embedded in silty sand soils deposited during the transgression-regression marine cycles that occurred after the last glacial episode. These soils are known for their poor mechanical properties and medium swelling index measured for some laboratory tests (Ruggeri et al., 2021).

To assess the role of seasonal groundwater level fluctuations, continuous groundwater monitoring data are essential (Figure 22b). For this purpose, we utilized the FaldaNET-ER database that provides monitoring data for shallow groundwater levels in the unconfined aquifer (phreatic water) located just a few meters below ground level (b.g.l.). Furthermore, daily cumulative rainfall data have been extracted from the ARPAE database (https://simc.arpae.it/dext3r/)

Our comparative analysis reveals a correlation between the seasonal trends observed in rainfall data, land displacements, and shallow groundwater level fluctuations. Consequently, we hypothesize that the observed seasonal movement in LH IC3 may be influenced by hydro-meteorological changes, as well as irrigation and drainage practices managed by the water reclamation authorities of the area (Figure 22c).
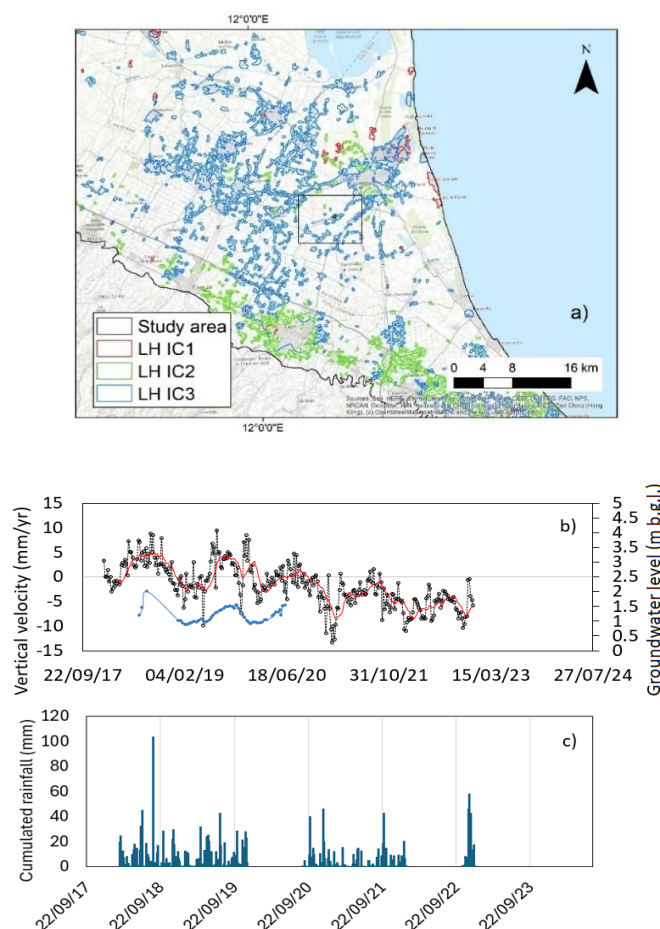


*Figure 22 – a) Location of the LH ICs in Ravenna province. b) Comparison between the displacement time series of measuring points in the LH IC3 indicated in the black box with the groundwater monitoring station available in the same LH IC3. The*

![MISSIONE 4 ISTRUZIONE RICERCA]

![SubRISK+ — Enhancing our understanding of Subsidence RISK induced by groundwater exploitation towards sustainable urban development]

*groundwater data is provided by FaldaNET-ER database (https://faldanet.consorziocer.it/).c) Daily rainfall data recorded by 14RA weather station located in Ravenna.*

### 3.2.5. Infrastructures/structures loading

Local effects due to infrastructure/structure loading have been evaluated by verifying the intersection between the Copernicus Corine Land Cover Changes (CLC) 1990-2000 (https://land.copernicus.eu/en) and the LH. The focus was on transformation from natural/agricultural areas to urban and rural areas, and LH IC1 and LH IC2 with average mean velocity higher than -3 mm/yr. In the entire study area, almost 9300 ha have been converted, mainly from agricultural lands to urban settlements (Figure 23). These areas are evenly distributed across the study area, with the highest occurrence in the western part. Considering only areas that lie in the LH IC1 and LH IC2, a few hotspots have been detected with a total coverage of 5.78 km$^2$, mainly in the Modena, Piacenza, Reggio Emilia and Ferrara provinces.
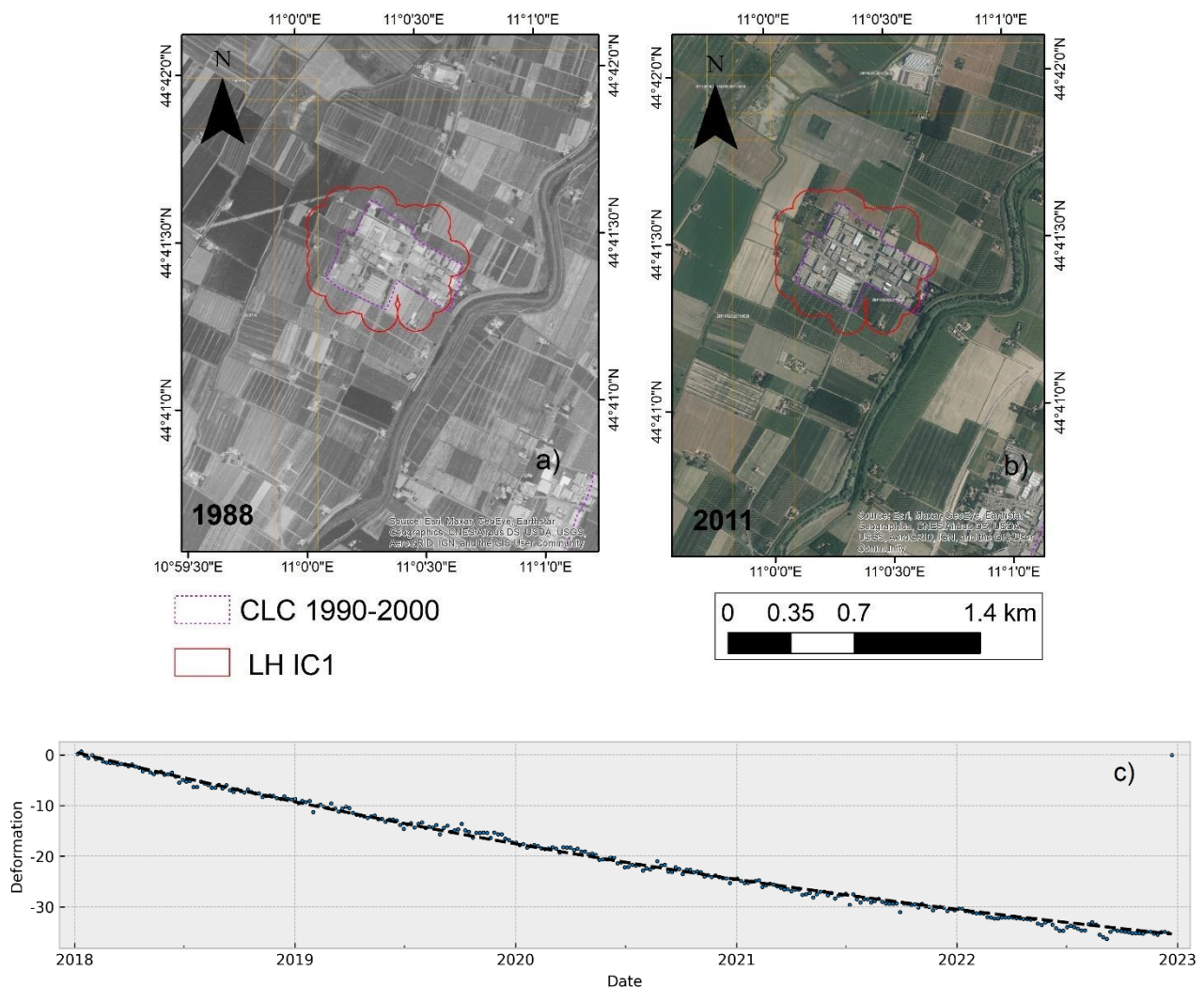


*Figure 23 – Example of the Land Cover changes from 1990 to 2000 and LH IC1 in Modena province. a) Overview of the 1988 and b) 2011 orthophotos. Source: https://gn.mase.gov.it/portale/servizio-di-consultazione-wms. c) Displacement versus time of one measuring point located within the LH IC1.*

MISSIONE 4
ISTRUZIONE
RICERCA

SubRISK+

Enhancing our understanding of Subsidence RISK induced by
groundwater exploitation towards sustainable urban development

### 3.2.6. Hydrocarbon storage and production

Usually, underground gas storage plants are characterized by a seasonal behavior of $CH_4$ injection and production, resulting in reservoir compaction and expansion, which are evident in terms of seasonal subsidence and rebound of the land surface above the reservoir. Therefore, a cross-comparison between the LH IC3 and the gas storage concession sites has been performed. Moreover, the LH IC1 and LH IC2 have been cross-compared with the gas production concession sites. The results of the analysis show that some local LH IC3 are detected in areas of gas storage concessions (Figure 24), such as the Minerbio site.
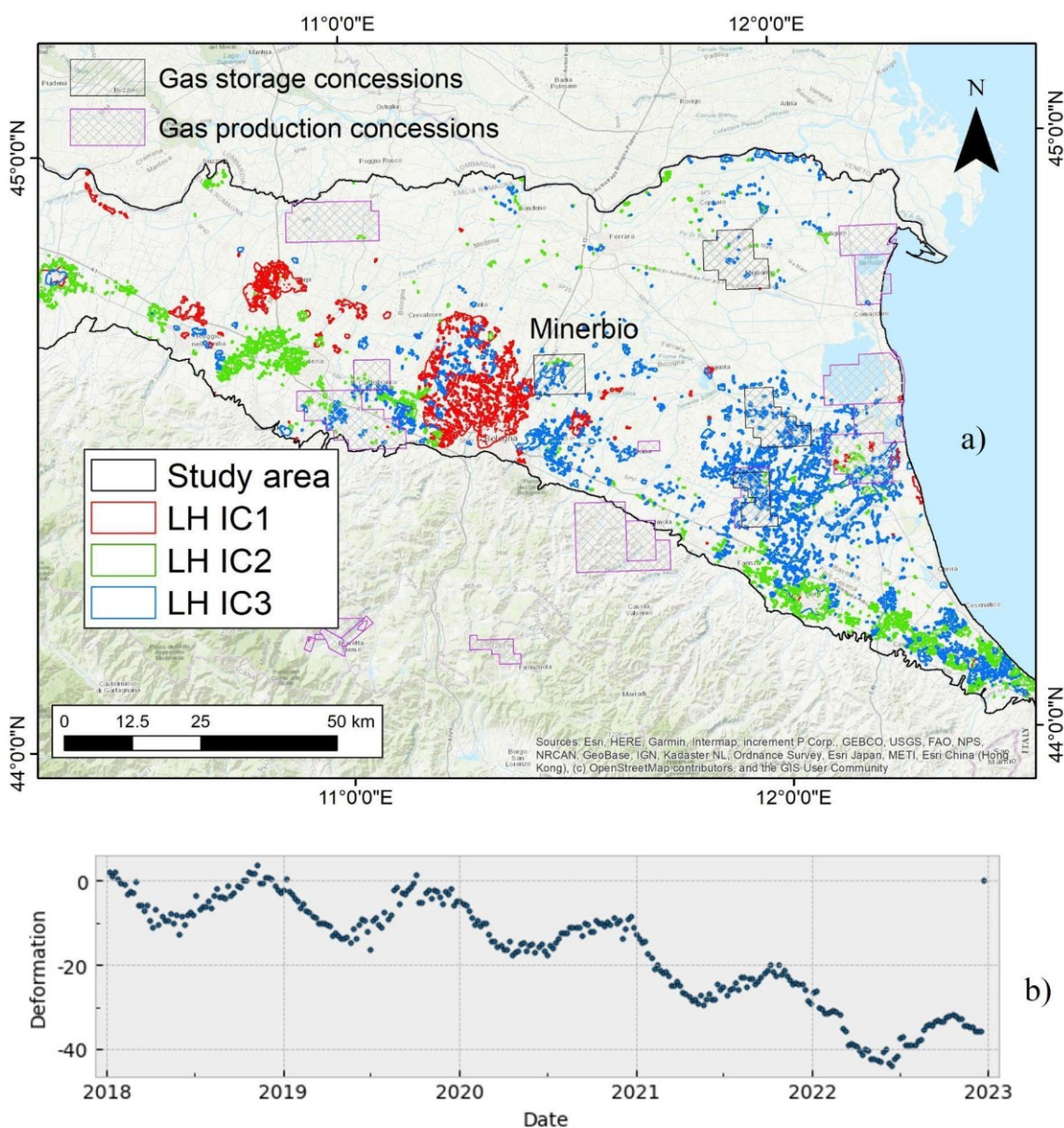


*Figure 24 – a) Location of the gas storage and production concessions. Source: https://dati.arpae.it/. b) Deformation trend extracted in the LH IC3 of the Minerbio site.*

## 3.3. Differential displacement risk in Emilia-Romagna region

The hazard assessment for the 9 provinces of Emilia-Romagna region depicts low hazard levels (H1) across more than 92.7 % of the mapped area of the building footprints (Figure 25); overall, the greatest proportion of medium (H2) to very high (H4) hazard zones is found in Bologna, where hazard is deemed significant across more than 6% of the mapped building coverage. In terms of absolute extent, Bologna (~3.2 km$^2$), Ravenna (~3.1 km$^2$), Ferrara (~1.9 km$^2$) and Modena (2.25 km$^2$) provide the greatest extents of H2 to H4 hazard zones, while the lowest extents are found in Piacenza (~0.62 km$^2$) and Rimini (~0.24 km$^2$). The hazard levels H3 and H4 are generally limited to small sectors of the region and encompass a total of 1.24 km$^2$ across the whole 9 provinces. It is worth noting that Ravenna, Ferrara, and Bologna are the provinces experiencing the greatest hazard level (H3 and H4), in a few spots with an area of 0.36, 0.22, and 0.16 km$^2$, respectively.
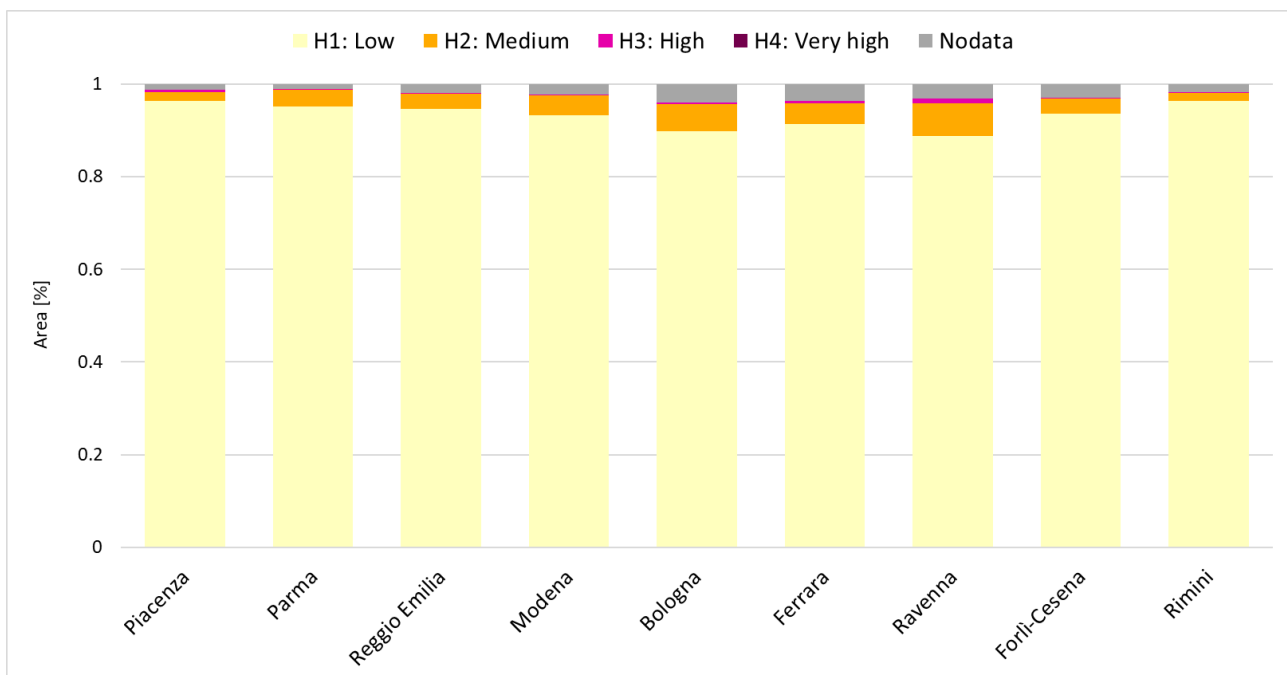


*Figure 25 – Extent of the four Hazard (H) classes within the 9 provinces of Emilia-Romagna region of Italy, displayed using a percentage scale (100% refers to the total extent of the hazard data within each district), and derived by following the method described in section 2.2.3.*

The proportion of building footprint area with low exposure-vulnerability buildings (EV1) within the Emilia-Romagna region is generally between 0.5% (found at Modena) and 2.2% (Forli-Cesena) and is not very evident with respect to the other classes (Figure 26). The building footprint area with medium exposure-vulnerability buildings (EV2) typically covers between 13.3% (Rimini) and 25.7% (Ferrara). Larger proportions are found for high exposure-vulnerability buildings (EV3), extending between 56.2% (Ferrara) and 65.8% (Piacenza). The building footprint area with the highest exposure-vulnerability metric (EV4) ranges between 3.5% (Ferrara) and 10.8% (Bologna). In terms of absolute extent, the provinces highlighting the largest extents of EV4 buildings footprints are Bologna (~5.7 km$^2$), Reggio Emilia (~2.9 km$^2$), and Modena (~2.8 km$^2$).
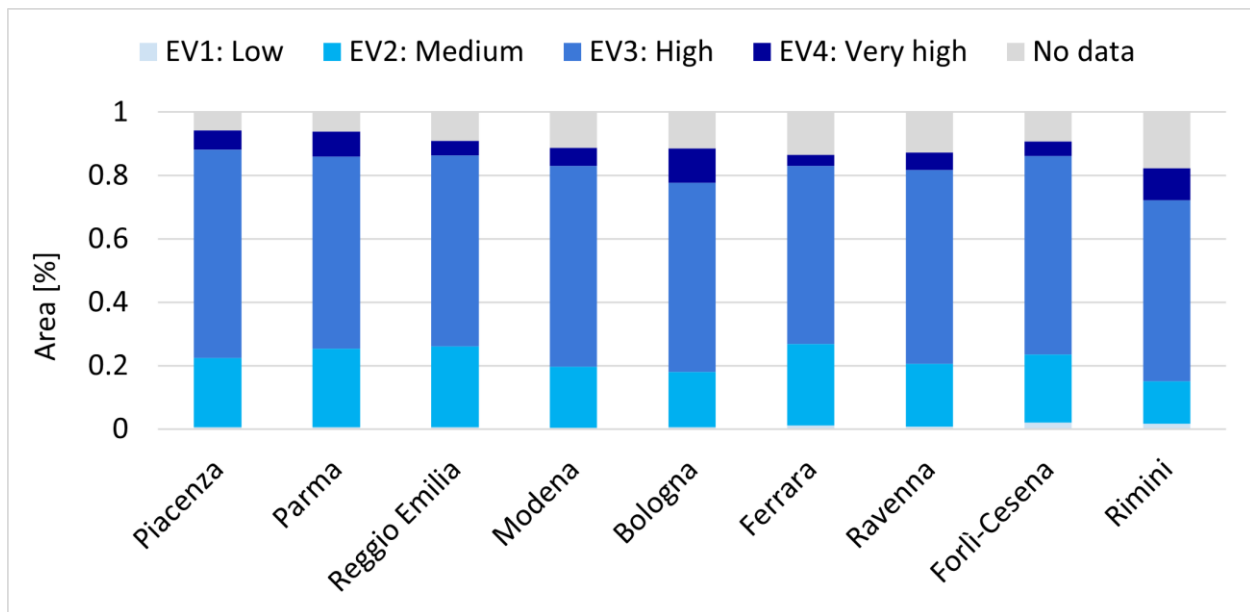
*Figure 26 – Extent of the four Exposure-Vulnerability (EV) levels within the 9 provinces of Emilia-Romagna Region of Italy, derived by following the method described in section 2.2.3.*

Regarding the differential displacement map of the Emilia-Romagna region, low risk (R1) zones cover ~14-25% of the area of the building footprint, with peaks at Reggio Emilia (~25.3%) and Parma (24.6%); medium risk (R2) areas typically extend (~60-72%), with peaks at Piacenza (72%) and Bologna (70%) (Figure 27). A total of 71.6 km$^2$ R1 and 227.3 km$^2$ R2 areas are found overall across the region.

On the other hand, a total of 1.7 km$^2$ high-risk (R3) zones are found overall across the 9 provinces. The highest risk level (R4) covers ~0.08 km$^2$, which is mostly limited to Ravenna and Bologna. More significant extents of R3 and R4 are found in Ravenna (0.71 km$^2$), Bologna (0.44 km$^2$), and Ferrara (0.15 km$^2$), in areas where the most vulnerable urban infrastructures are to the greatest differential settlements and induced structural stress (see section 2.2.3).

The risk map for each province has been shown in the following section (see sections 3.3.1- 3.3.9).
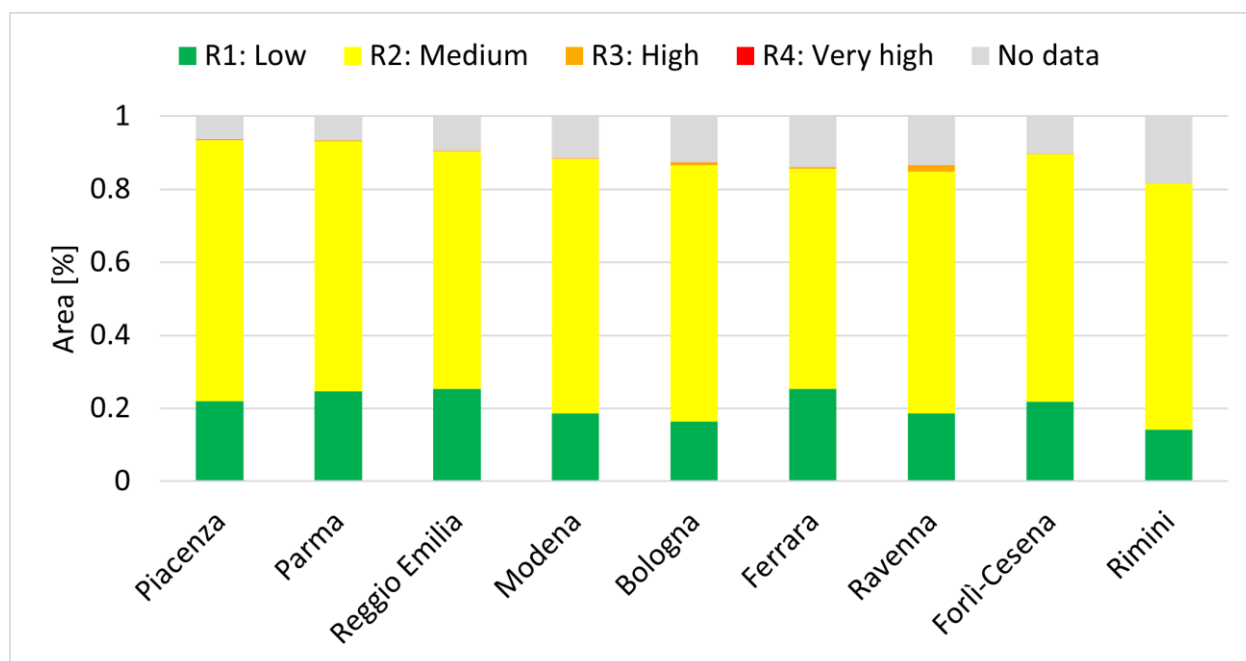
*Figure 27 – Extent of the four Risk (R) classes within each of the 9 provinces of Emilia-Romagna, derived by following the method described in section 2.2.3.*

### 3.3.1. Piacenza



*Figure 28 – Extent of the four Risk (R) classes within the province of Piacenza.*

### 3.3.2. Parma



*Figure 29– Extent of the four Risk (R) classes within the province of Parma.*

### 3.3.3. Reggio Emilia



*Figure 30– Extent of the four Risk (R) classes within the province of Reggio Emilia.*

### 3.3.4. Modena



*Figure 31– Extent of the four Risk (R) classes within the province of Modena.*

### 3.3.5. Bologna



*Figure 32– Extent of the four Risk (R) classes within the province of Bologna.*

### 3.3.6. Ferrara



*Figure 33– Extent of the four Risk (R) classes within the province of Ferrara.*

### 3.3.7. Ravenna



*Figure 34– Extent of the four Risk (R) classes within the province of Ravenna,*

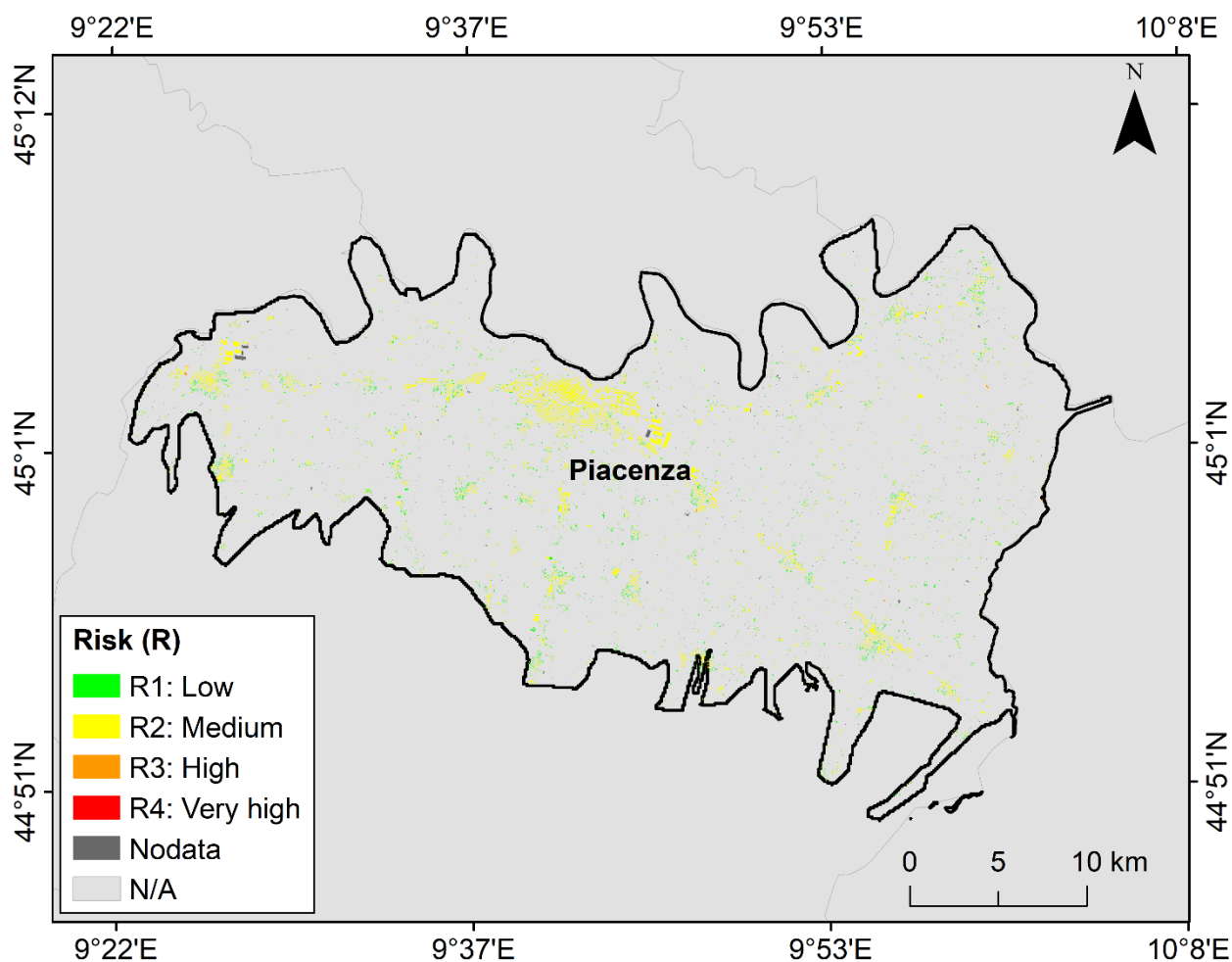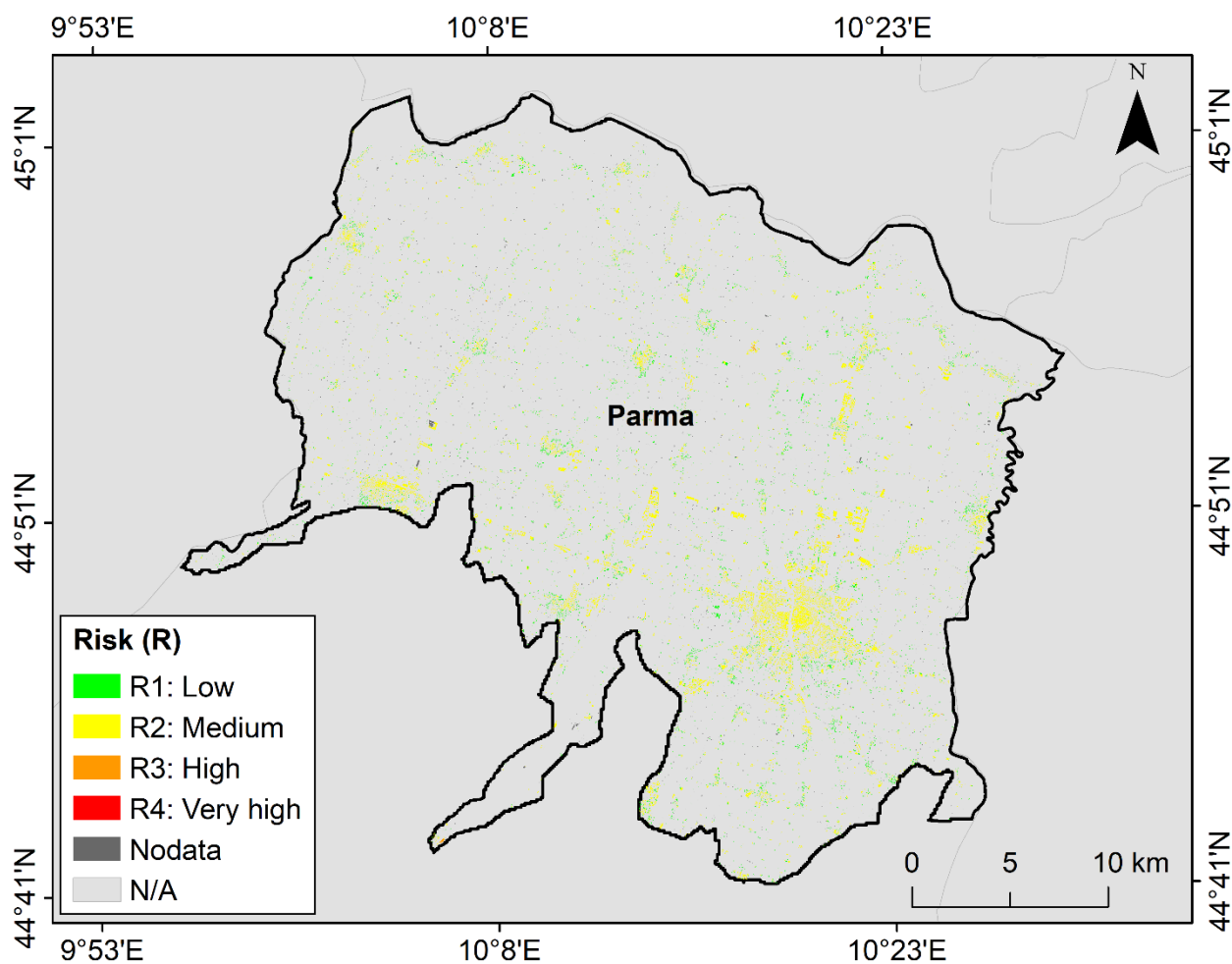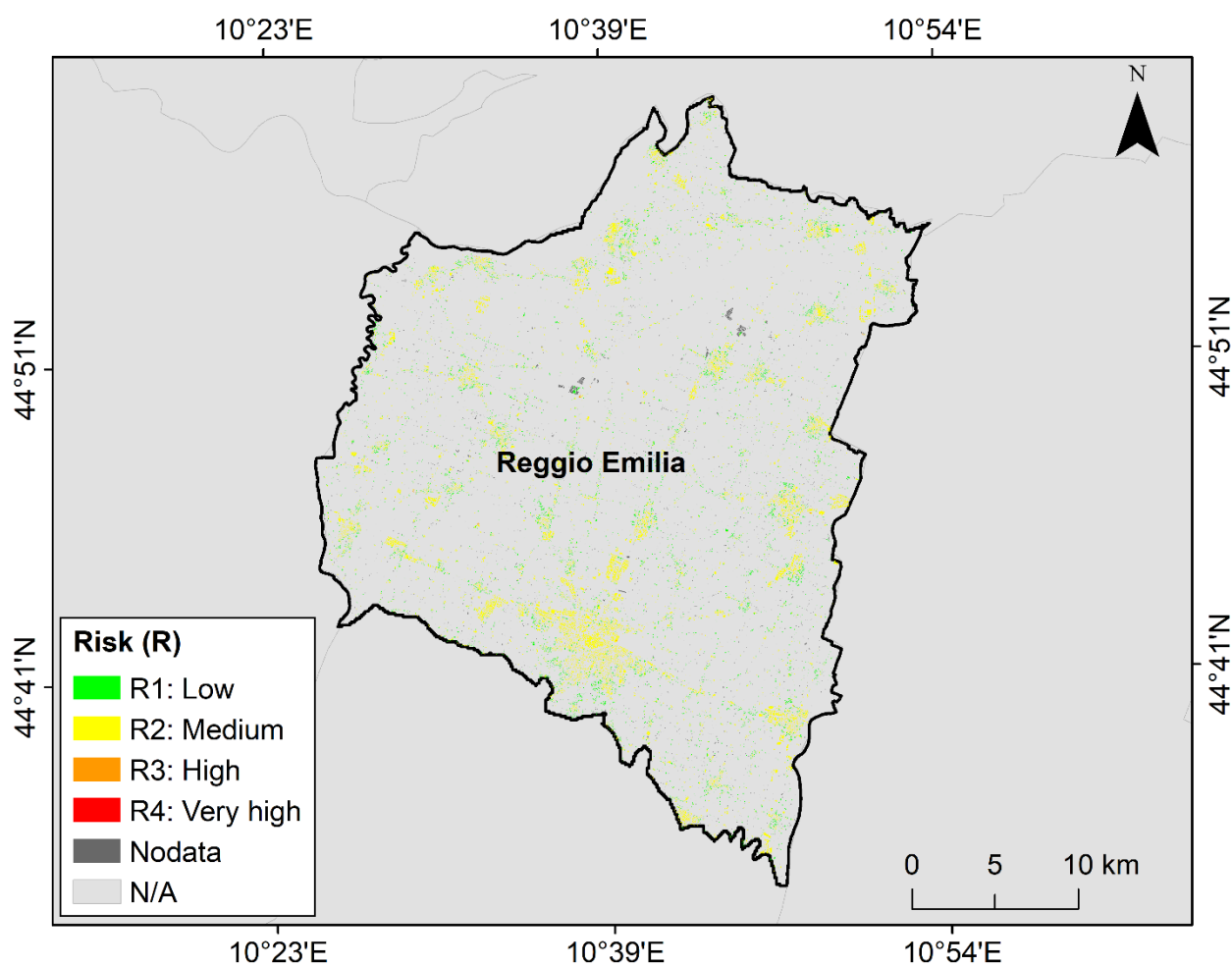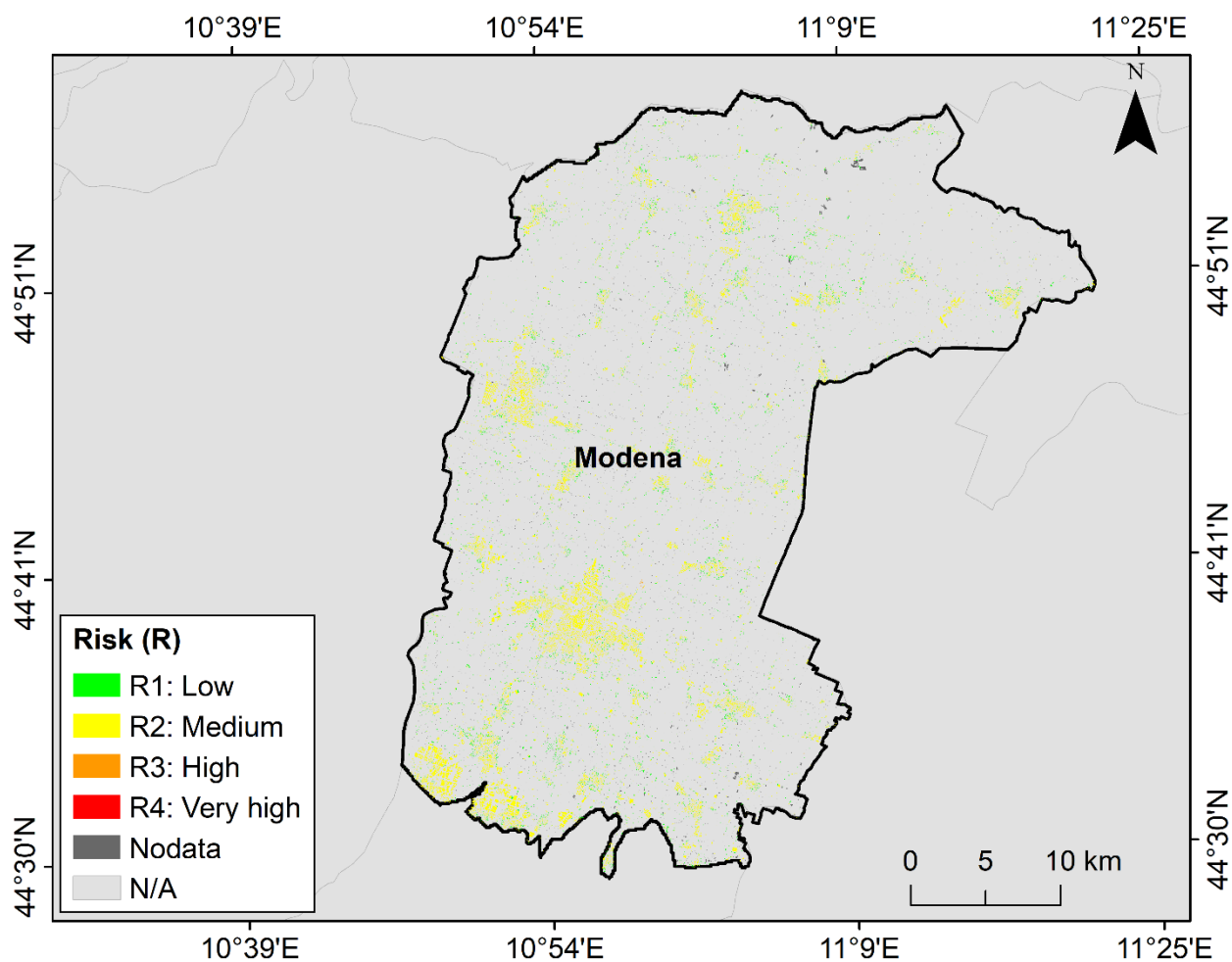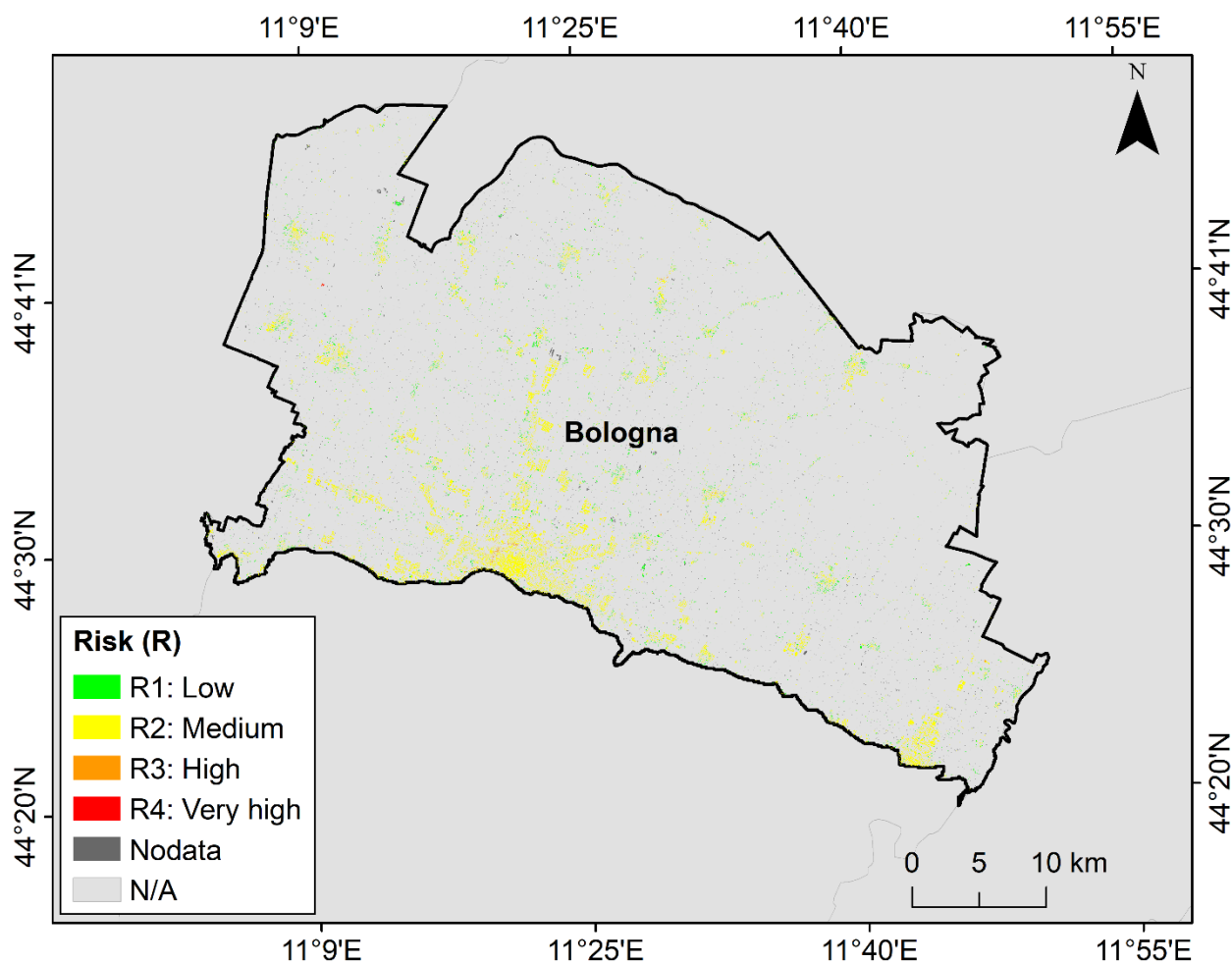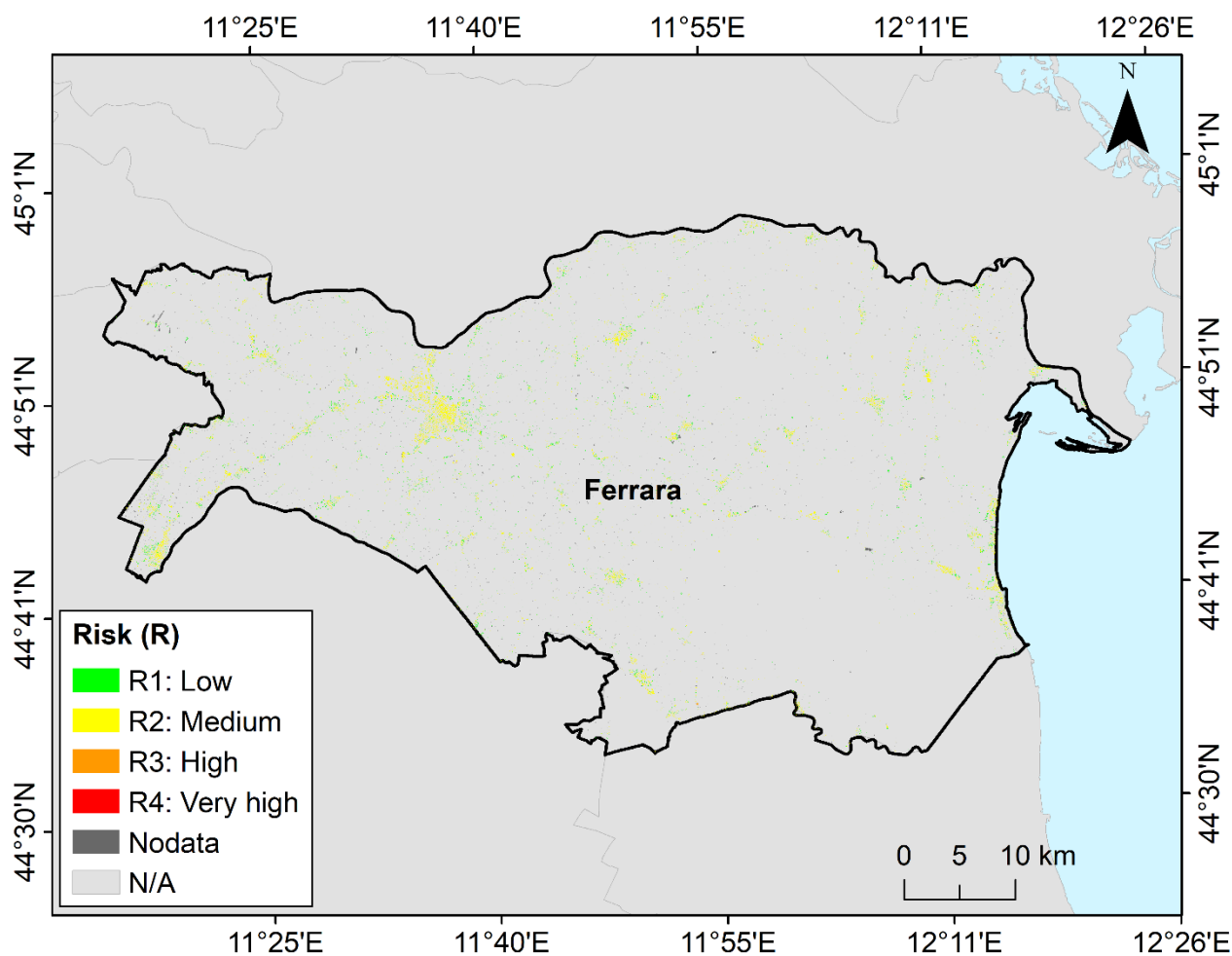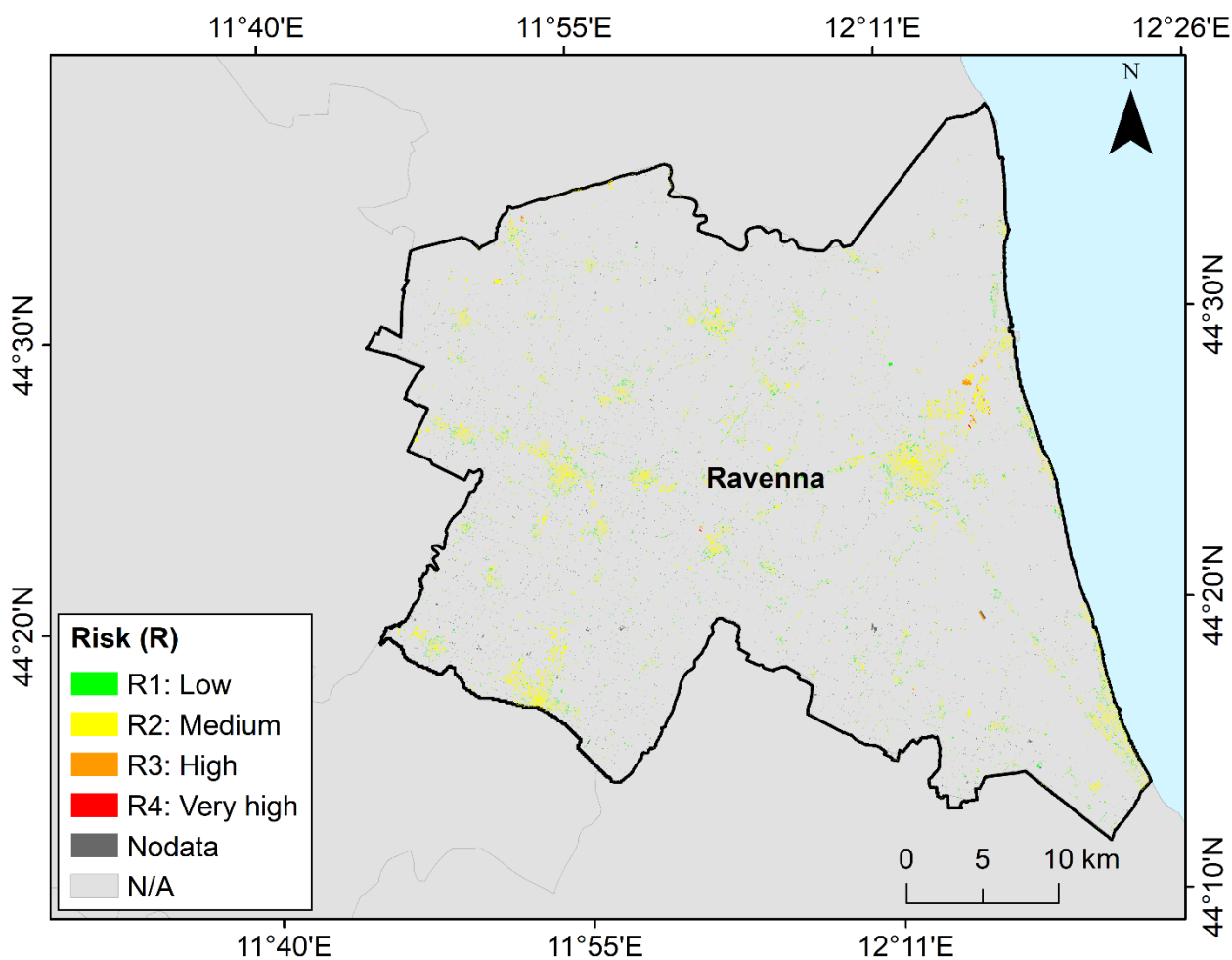### 3.3.8. Forlì-Cesena
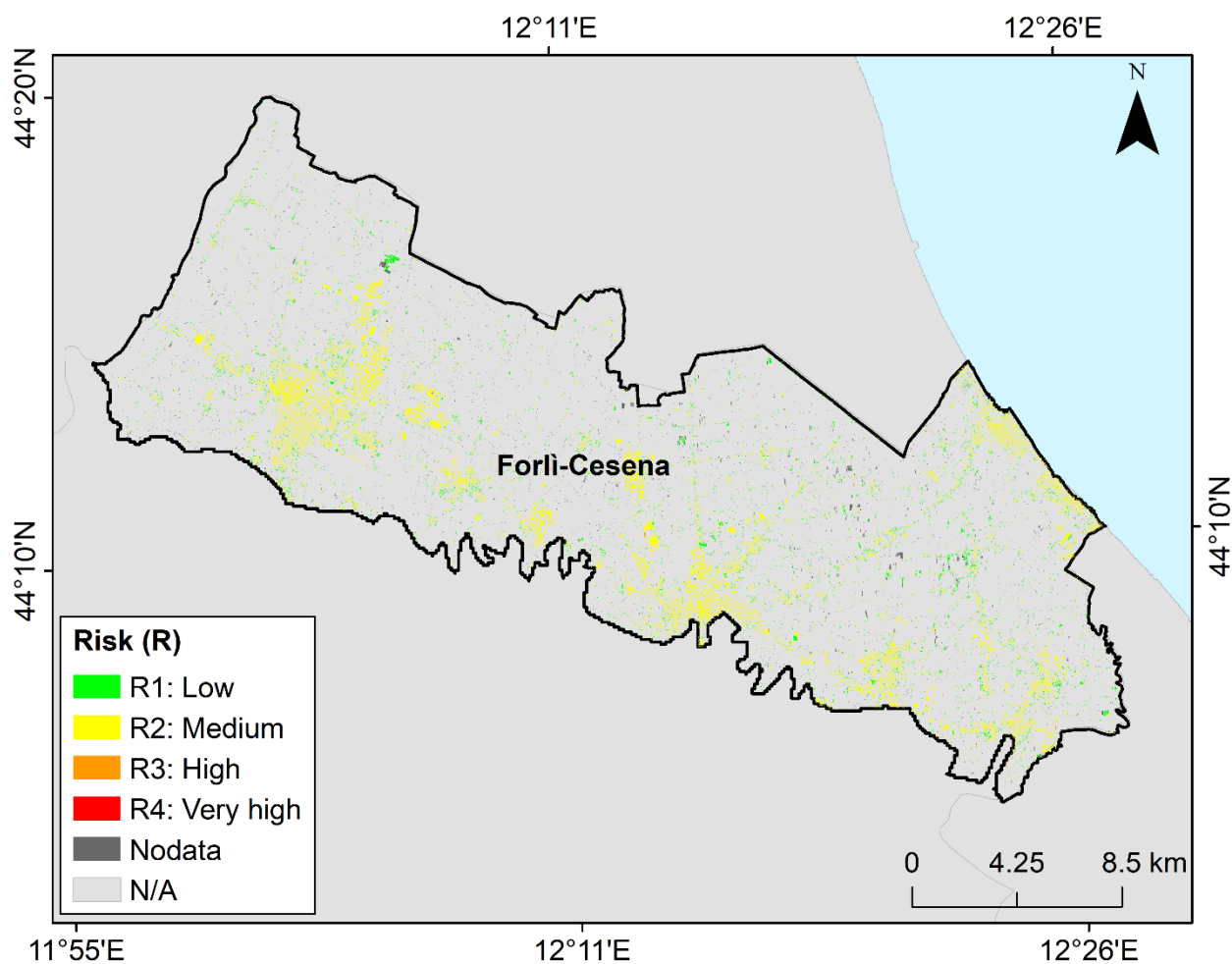


*Figure 35– Extent of the four Risk (R) classes within the province of Forlì-Cesena.*

### 3.3.9. Rimini
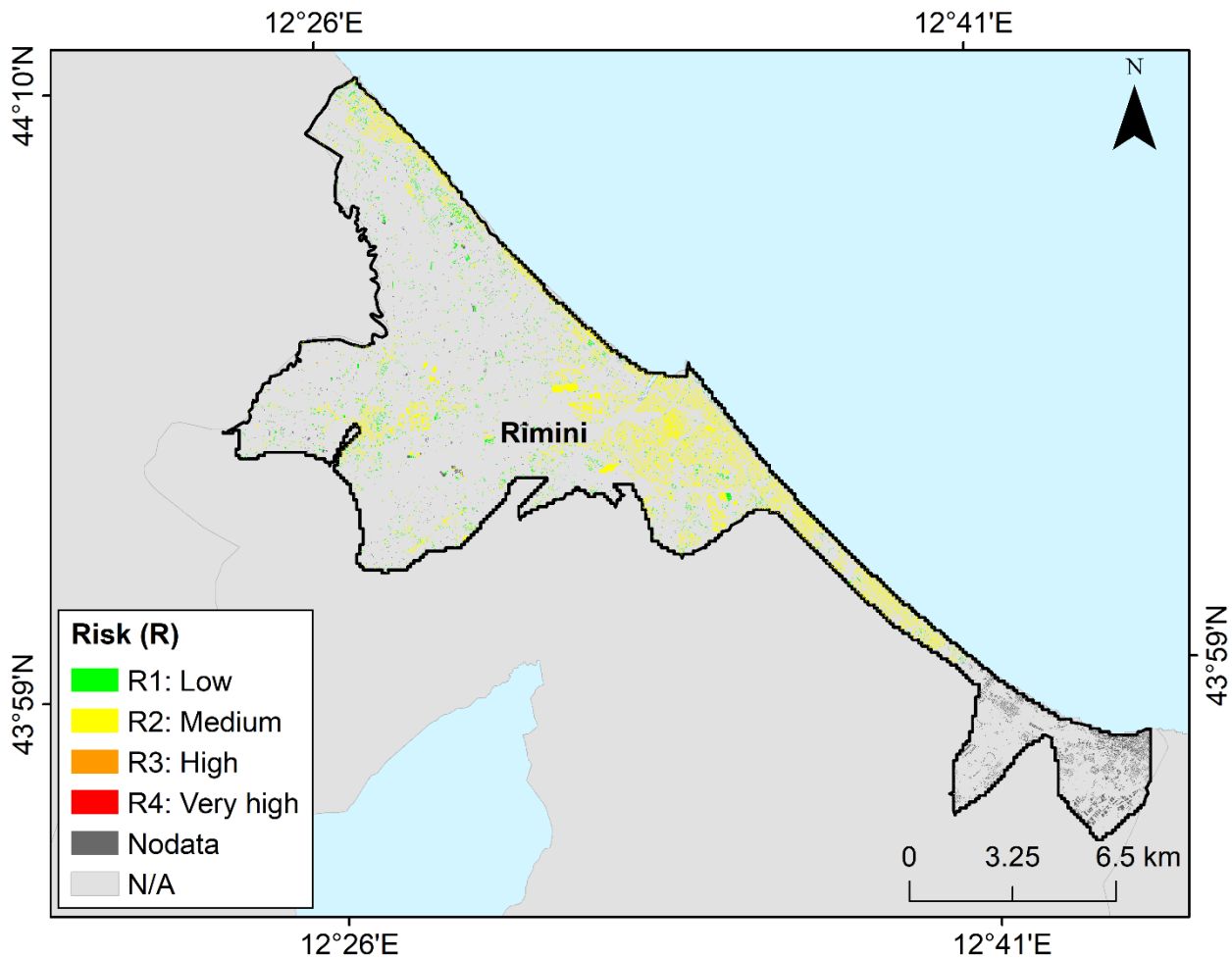


Figure 36– Extent of the four Risk (R) classes within the province of Rimini.

## 4. CONCLUSIONS

The investigation on land subsidence in the Emilia-Romagna region provided an overview of the extent and location of land displacement hotspots across over 10.000 km$^2$ from 2018 to 2022. The hotspots in the Emilia-Romagna region show different temporal trends, including linear, non-linear, and seasonal behavior. The maximum land subsidence rates are observed in Bologna, reaching values exceeding -30 mm/yr over an area of more than 130 km$^2$. The most extended hotspots of the first independent component, i.e. a mainly linear trend, are observed in the Reggio Emilia and Bologna provinces. The non-linear trend is mainly localized in proximity to the Apennine alluvial fans, whereas seasonal movements were detected mainly in Ravenna province. Evidences of natural causes of land subsidence due to compaction of recent alluvial soils and tectonic movements were recognised. Anthropogenic factors such as the groundwater withdrawal from confined or semi-confined aquifers, seasonal surface water management associated to meteorologic conditions, hydrocarbon production, gas storage, and infrastructure/structures loading have been evidenced as well.

Regarding the differential displacement risk mapping, high and very high levels of risk were identified across 1.8 km². The study area is mainly under a medium risk level, with the extent of ~60-71% in each province. The highest risk levels (R3 and R4) are mostly limited to the Ravenna and Bologna provinces.

When using hotspot and risk mapping products provided in this report and in the SubRISK+ Control Room digital platform, consider the following:

- The spatial resolution of 100 m resolution of the input EGMS Ortho layers affects the detection of the clusters of the LH database. It is worth noting that zones of low coherence, such as vegetated areas (e.g., Ferrara province), are also known to hinder the exploitation of InSAR data due to the lower density of measuring points. Integration between satellite, in situ data (e.g. levelling, GNSS), and artificial corner reflectors might improve the monitoring over areas with few natural coherent reflectors.

- The input EGMS Ortho layers do not provide information on N-S displacement that may occur, hence horizontal strain along the N-S direction is not accounted for; in such cases, other geodetic data (e.g., GPS/GNSS) might provide complementary data to enhance the detection of the ground displacement hotspots and the hazard assessment in the risk analysis. Future Earth Observation (EO) products, such as those offered by the IRIDE program will provide some solution to measure the North-South deformation component using the NIMBUS X-Band synthetic aperture radar (SAR) IRIDE subconstellation characterized by a mid-inclination orbits (Cotugno et al. 2024).

- The LH does not represent geohazards; therefore, their geological interpretation requires ancillary data to investigate in detail the areas. The LH may be influenced by local factors, such as thermal deformation of the targets on the ground surface, or issues due to the interferometric method itself (e.g., outliers, phase unwrapping errors).

- The investigation of the drivers is influenced by the availability of the ancillary data, and the main causes are here preliminarily investigated for the entire Emilia-Romagna region. Therefore, local-scale analyses should be performed to investigate each area in detail, starting from a geotechnical model of the LH. Further information about the aquifer compaction layers might be improved using in situ monitoring systems such as extensometers.

- The spatial resolution of the differential displacement risk maps is influenced by the resolution of the input datasets that are exploited to generate them, namely: hazard mapping is performed at the same 100 m resolution of the input EGMS Ortho layers, while exposure-vulnerability mapping is based on the 10 m resolution provided by GHSL. The building footprints are then used as spatial reference for the risk assessment, meaning that the input hazard information associated with each pixel is homogeneous across 100 m by 100 m areas, and input exposure-vulnerability data refer to 10 m by 10 m pixels. Hence, smaller (e.g. building-specific) spatial granularities are not accounted for.

- The differential settlement risk mapping does not include information on building and foundation typology, maintenance status, or other structural health parameters of the buildings that may influence their vulnerability. A detailed analysis of such parameters at the building-block or building scale would be recommended to enhance the assessment at finer analysis scales. The outcomes provide a starting point for conducting further field surveys to evaluate

damage to buildings and for more detailed geological and geotechnical investigations at specific sites.

- The hazard mapping approach assumes that the estimated land displacement velocities for the 2018–2022 period have affected the observed areas for a total of 30 years (namely, during 1993–2022). This assumption may result in an underestimation of hazard levels for areas affected by subsidence processes for more than the selected 30-year-long interval, and an overestimation of hazard levels for areas affected for shorter periods.

- The hazard mapping is estimated considering a total angular distortion and strain constant in the 30-year-long interval. No accelerations and decelerations are considered in this analysis.

- The differential settlement risk mapping only refers to the building footprints. Hence, risk levels are not provided for other areas, such as linear infrastructures (e.g., roads, railways, pipelines, and power lines) and irrigation channels. Furthermore, the level of risk does not account for land subsidence magnitude, which can result in amplified topographic depressions or increased flooding impact in fluvial systems and coastal areas.

# 5. References

Amorosi, A., & Marchi, N. (1999). High-resolution sequence stratigraphy from piezocone tests: an example from the Late Quaternary deposits of the southeastern Po Plain. Sedimentary Geology, 128(1-2), 67-81.

Amorosi, A., Farina, M., Severi, P., Preti, D., Caporale, L. and Di Dio, G., 1996. Genetically related alluvial deposits across active fault zones: an example of alluvial fan-terrace correlation from the upper Quaternary of the southern Po Basin, Italy. *Sedimentary Geology*, *102*(3-4), pp.275-295.

Baldi, P., Casula, G., Cenni, N., Loddo, F. and Pesci, A., 2009. GPS-based monitoring of land subsidence in the Po Plain (Northern Italy). *Earth and Planetary Science Letters*, *288*(1-2), pp.204-212.

Barra, A., Reyes-Carmona, C., Herrera, G., Galve, J. P., Solari, L., Mateos, R. M., ... & Monserrat, O. (2022). From satellite interferometry displacements to potential damage maps: A tool for risk reduction and urban planning. Remote Sensing of Environment, 282, 113294.

Baú, D., Gambolati, G., & Teatini, P. (2000). Residual land subsidence near abandoned gas fields raises concern over northern Adriatic coastland. Eos, Transactions American Geophysical Union, 81(22), 245-249.

Bitelli, G., Bonsignore, F. and Unguendoli, M., 2000. Levelling and GPS networks to monitor ground subsidence in the Southern Po Valley. *Journal of Geodynamics*, *30*(3), pp.355-369.

Boccaletti, M., Corti, G. and Martelli, L., 2011. Recent and active tectonics of the external zone of the Northern Apennines (Italy). *International Journal of Earth Sciences*, *100*(6), pp.1331-1348.

Bonì, R., Pilla, G. and Meisina, C., 2016. Methodology for detection and interpretation of ground motion areas with the A-DInSAR time series analysis. *Remote Sensing*, *8*(8), p.686.

Bruno, L., Campo, B., Costagli, B., Stouthamer, E., Teatini, P., Zoccarato, C., & Amorosi, A. (2020). Factors controlling natural subsidence in the Po Plain. Proceedings of the International Association of Hydrological Sciences, 382, 285-290.

Burland, J.B.; Wroth, C.P. Settlement of Buildings and Associated Damage. In Proceedings of the SOA Review, Proc. Conf. Settlement of Structures, Pentech Press, Cambridge, London; 1974; pp. 611–654.

Caputo, M., Pieri, L. and Unguendoli, M., 1970. Geometric investigation of the subsidence in the Po Delta. CNR, Laboratorio per lo studio della dinamica delle grandi masse.

Carbognin, L., Gatto, P., & Mozzi, G. (1984). Case history no. 9.15: Ravenna, Italy. Guidebook to Studies of Land Subsidence due to Ground-Water Withdrawal; Poland, J. F. (Ed.), 291-305.

Carydis, P., Castiglioni, C., Lekkas, E., Kostaki, I., Lebesis, N. and Drei, A., 2012. The Emilia-Romagna, May 2012 earthquake sequence. The influence of the vertical earthquake component and related geoscientific and engineering aspects. *Ingegneria Sismica*, *29*(2-3), pp.31-58.

Carminati, E. and Martinelli, G., 2002. Subsidence rates in the Po Plain, northern Italy: the relative impact of natural and anthropogenic causation. *Engineering Geology*, *66*(3-4), pp.241-255.

Carminati, E. and Doglioni, C., 2012. Alps vs. Apennines: The paradigm of a tectonically asymmetric Earth. *Earth-Science Reviews*, *112*(1-2), pp.67-96.

Castaldini, D., Marchetti, M., Norini, G., Vandelli, V. and Zuluaga Vélez, M.C., 2019. Geomorphology of the central Po Plain, Northern Italy. *Journal of Maps*, *15*(2), pp.780-787.

CEN *Eurocode 7: Geotechnical design - Part 1: General rules [EN 1997-1]. Authority: The European Union Per Regulation 305/2011, Directive 98/34/EC, Directive 2004/18/EC.*; 2004;

Ciavola, P., Corbau, C., Cibin, U. and Perini, L., 2003, October. Mapping of the coastal zone of the Emilia-Romagna region using geographical information systems. In *Proceedings of the Sixth International Conference on the Mediterranean Coastal Environment (MEDCOAST)* (Vol. 3, pp. 2363-2374). MEDCOAST Ravenna, Italy.

Cigna, F., Osmanoğlu, B., Cabral-Cano, E., Dixon, T. H., Ávila-Olivera, J. A., Garduño-Monroy, V. H., ... & Wdowinski, S. (2012). Monitoring land subsidence and its induced geological hazard with Synthetic Aperture Radar Interferometry: A case study in Morelia, Mexico. Remote Sensing of Environment, 117, 146-161.

Cigna, F.; Tapete, D. Present-day land subsidence rates, surface faulting hazard and risk in Mexico City with 2014–2020 Sentinel-1 IW InSAR. *Remote Sens. Environ.* 2021-a, *253*, 1–19, doi:10.1016/j.rse.2020.112161.

Cigna, F.; Tapete, D. Satellite InSAR survey of structurally-controlled land subsidence due to groundwater exploitation in the Aguascalientes Valley, Mexico. *Remote Sens. Environ.* 2021-b, *254*, 1–23, doi:10.1016/j.rse.2020.112254.

Cigna, F.; Tapete, D. Urban growth and land subsidence: Multi-decadal investigation using human settlement data and satellite InSAR in Morelia, Mexico. *Sci. Total Environ.* 2022, *811*, 152211, doi:10.1016/j.scitotenv.2021.152211.

Cigna, F., Paranunzio R., Bonì, R. & Teatini P. (2024). PRIN 2022 PNRR SubRISK+ Deliverable DEL 2.2: Present-day land subsidence risk in Italy, Version 1.0, Issue date: 30/09/2024, pp. 67. Public Report.

Conti, F., Eugeni, M., Bove, M., Marzioli, P., Marini, L., Pasquali, M., ... & Gaudenzi, P. (2024). A Model-based approach for the preliminary design of the SAR Upstream element for the Italian IRIDE EO constellation based on users' demand. CEAS Space Journal, 1-23.

Cotugno, F., Berardino, P., Bonano, M., Ciccolella, A., Costa, G., Crespo, F. M., ... & Lanari, R. (2024). Constellation design and analysis for spaceborne DInSAR mapping in mid inclination orbits: The IRIDE NIMBUS mission. IEEE Transactions on Geoscience and Remote Sensing.

Crosetto, M.; Solari, L.; Mróz, M.; Balasis-Levinsen, J.; Casagli, N.; Frei, M.; Oyen, A.; Moldestad, D.A.; Bateson, L.; Guerrieri, L.; et al. The evolution of wide-area DInSAR: From regional and national services to the European ground motion service. *Remote Sens.* 2020, *12*, 2043, doi:10.3390/RS12122043.

DISS Working Group, Database of Individual Seismogenic Sources (DISS), version 3.3.1: A compilation of potential sources for earthquakes larger than M 5.5 in Italy and surrounding areas. 2025, March 28. Istituto Nazionale di Geofisica e Vulcanologia (INGV). https://doi.org/10.13127/diss3.3.1

Eid, C., Benetatos, C. and Rocca, V., 2022. Fluid production dataset for the assessment of the anthropogenic subsidence in the Po Plain area (Northern Italy). *Resources*, *11*(6), p.53.

Fiaschi, S., Tessitore, S., Bonì, R., Di Martire, D., Achilli, V., Borgstrom, S., ... & Calcaterra, D. (2017). From ERS-1/2 to Sentinel-1: Two decades of subsidence monitored through A-DInSAR techniques in the Ravenna area (Italy). GIScience & Remote Sensing, 54(3), 305-328.

Gaddes, M.E., Hooper, A., Bagnardi, M., Inman, H. and Albino, F., 2018. Blind signal separation methods for InSAR: The potential to automatically detect and monitor signals of volcanic deformation. *Journal of Geophysical Research: Solid Earth*, *123*(11), pp.10-226.

Gambolati, G., Giunta, G., Putti, M., Teatini, P., Tomasi, L., Betti, I., ... & Gonella, M. (1998). Coastal evolution of the Upper Adriatic Sea due to sea level rise and natural and anthropic land subsidence. CENAS: coastline evolution of the upper adriatic sea due to sea level rise and natural and anthropogenic land subsidence, 1-34.

Gambolati, G., Ricceri, G., Bertoni, W., Brighenti, G., & Vuillermin, E. (1991). Mathematical simulation of the subsidence of Ravenna. Water Resources Research, 27(11), 2899-2918.

Gambolati, G., Teatini, P., Tomasi, L., & Gonella, M. (1999). Coastline regression of the Romagna region, Italy, due to natural and anthropogenic land subsidence and sea level rise. Water Resources Research, 35(1), 163-184.

Jolliffe, I.T., 1990. Principal component analysis: a beginner's guide—I. Introduction and application. *Weather*, *45*(10), pp.375-382.

Marcaccio, M. and Martinelli, G., 2012. Effects on the groundwater levels of the May-June 2012 Emilia seismic sequence. *Annals of Geophysics*, *55*(4).

Marconcini, M.; Metz-Marconcini, A.; Üreyen, S.; Palacios-Lopez, D.; Hanke, W.; Bachofer, F.; Zeidler, J.; Esch, T.; Gorelick, N.; Kakarla, A.; et al. Outlining where humans live, the World Settlement Footprint 2015. *Sci. Data* 2020, *7*, 1–14, doi:10.1038/s41597-020-00580-5.

Marchetti, M., 2002. Environmental changes in the central Po Plain (northern Italy) due to fluvial modifications and anthropogenic activities. *Geomorphology*, *44*(3-4), pp.361-373.

Martelli, L., Severi, P., Biavati, G., Rosselli, S., Camassi, R., Ercolani, E., Marcellini, A., Tento, A., Gerosa, D., Albarello, D. and Guerrini, F., 2014. Analysis of the local seismic hazard for the stability tests of the main bank of the Po river (Northern Italy). *Bollettino di Geofisica Teorica ed Applicata*, *55*(1).

Nespoli, M., Cenni, N., Belardinelli, M.E. and Marcaccio, M., 2021. The interaction between displacements and water level changes due to natural and anthropogenic effects in the Po Plain (Italy): The different point of view of GNSS and piezometers. *Journal of Hydrology*, *596*, p.126112.

Olivucci S., Nerieri M., Ruggieri G., Romani M., Ceresini S., Gentili G. Il nuovo strato Edificato da tecniche "deep learning" come fonte per l'aggiornamento del Database Topografico e per il monitoraggio del consumo di suolo. Asita 2019.

Ord, J.K.; Getis, A. Local Spatial Autocorrelation Statistics: Distributional Issues and an Application. Geogr. Anal. 1995, 27, 286–306.

Peduto, D.; Nicodemo, G.; Maccabiani, J.; Ferlisi, S. Multi-scale analysis of settlement-induced building damage using damage surveys and DInSAR data: A case study in The Netherlands. *Eng. Geol.* 2017, *218*, 117–133, doi:10.1016/j.enggeo.2016.12.018.

RER & ENI-Agip (1998) Riserve idriche sotterranee della Regione Emilia-Romagna. Edited by G. M. Di Dio. Regione Emilia-Romagna, ufficio geologico—ENI-Agip, Divisione Esplorazione & Produzione. S.EL.CA., Firenze, 120 pp.

Pesaresi, M.; Panagiotis, P. *GHS-BUILT-C R2023A - GHS Settlement Characteristics, derived from Sentinel2 composite (2018) and other GHS R2023A data. European Commission, Joint Research Centre (JRC)*;

Qu, F.; Zhang, Q.; Lu, Z.; Zhao, C.; Yang, C.; Zhang, J. Land subsidence and ground fissures in Xi'an, China 2005–2012 revealed by multi-band InSAR time-series analysis. *Remote Sens. Environ.* 2014, *155*, 366–376, doi:10.1016/J.RSE.2014.09.008.

Righini, M., Bonì, R., Sapio, S., Gatti, I., Salvadore, M. and Taramelli, A., 2024. Development of a Proof-of-Concept A-DInSAR-Based Monitoring Service for Land Subsidence. *Remote Sensing*, *16*(11), p.1981.

Ruggeri, P., Fruzzetti, V.M.E. and Scarpelli, G., 2021. Characterization of the recent soft silty clay deposit in the Ravenna port area (Italy). In *Proc., 6th Int. Conf. on Geotechnical and Geophysical Site Characterisation. London: International Society for Soil Mechanics and Geotechnical Engineering. https://doi. org/10.53243/ISC2020-210.*

Sanabria, M.P.; Guardiola-Albert, C.; Tomás, R.; Herrera, G.; Prieto, A.; Sánchez, H.; Tessitore, S. Subsidence activity maps derived from DInSAR data: Orihuela case study. *Nat. Hazards Earth Syst. Sci.* 2014, *14*, 1341–1360, doi:10.5194/nhess-14-1341-2014.

Skempton, A.W.; McDonalds, D.H. Allowable settlements of buildings. In Proceedings of the Proc. ICE, London, 5; 1956; pp. 727–768.

Taramelli, A., Di Matteo, L., Ciavola, P., Guadagnano, F., & Tolomei, C. (2015). Temporal evolution of patterns and processes related to subsidence of the coastal area surrounding the Bevano River mouth (Northern Adriatic)–Italy. *Ocean & Coastal Management*, *108*, 74-88.

Tandanand, S.; Powell, L.R. *Determining horizontal displacement and strains due to subsidence. Report of Investigations n.9358*; U.S. Department of the Interior, Bureau of Mines, 1991;

Teatini, P., Gambolati, G., Tomasi, L., & Putti, M. (1998). Simulation of land subsidence due to gas production at Ravenna coastline. CENAS: coastline evolution of the upper adriatic sea due to sea level rise and natural and anthropogenic land subsidence, 133-150.

Teatini, P., Ferronato, M., Gambolati, G. and Gonella, M., 2006. Groundwater pumping and land subsidence in the Emilia-Romagna coastland, Italy: Modeling the past occurrence and the future trend. *Water Resources Research*, *42*(1).

Zhu, M.; Wan, X.; Fei, B.; Qiao, Z.; Ge, C.; Minati, F.; Vecchioli, F.; Li, J.; Costantini, M. Detection of Building and Infrastructure Instabilities by Automatic Spatiotemporal Analysis of Satellite SAR Interferometry Measurements. *Remote Sens.* 2018, *10*, 1816, doi:10.3390/rs10111816.